Title
Quantifying fire-wide carbon emissions in interior Alaska using field measurements and Landsat imagery

Journal
Journal of Geophysical Research Biogeosciences, 119(8)

ISSN
2169-8953

Authors
Rogers, BM
Veraverbeke, S
Azzari, G
et al.

Publication Date
2014-08-01

DOI
10.1002/2014jg002657

AGU PUBLICATIONS

JGR

Journal of Geophysical Research: Biogeosciences

RESEARCH ARTICLE
10.1002/2014JG002657

Key Points:
- Fire emissions in Alaska were quantified with field and remote sensing data
- dNBR exhibits a clear and nonlinear relationship with combustion
- Field observations overestimate fire-wide combustion

Supporting Information:
- Readme
- Tables S1–S3 and Figures S1–S7

Correspondence to:
B. M. Rogers,
brogers@whrc.org

Citation:
Rogers, B. M., S. Veraverbeke, G. Azzari, C. I. Czimczik, S. R. Holden, G. O. Mouteva, F. Sedano, K. K. Treseder, and J. T. Randerson (2014), Quantifying fire-wide carbon emissions in interior Alaska using field measurements and Landsat imagery, *J. Geophys. Res. Biogeosci.*, *119*, 1608–1629, doi:10.1002/2014JG002657.

Received 27 FEB 2014
Accepted 18 JUL 2014
Accepted article online 23 JUL 2014
Published online 19 AUG 2014

Quantifying fire-wide carbon emissions in interior Alaska using field measurements and Landsat imagery

B. M. Rogers[1,2], S. Veraverbeke[1], G. Azzari[1], C. I. Czimczik[1], S. R. Holden[3], G. O. Mouteva[1], F. Sedano[4], K. K. Treseder[3], and J. T. Randerson[1]

[1]Department of Earth System Science, University of California, Irvine, California, USA, [2]Now at Woods Hole Research Center, Falmouth, Massachusetts, USA, [3]Department of Ecology and Evolutionary Biology, University of California, Irvine, California, USA, [4]Department of Geographical Sciences, University of Maryland, College Park, Maryland, USA

Abstract Carbon emissions from boreal forest fires are projected to increase with continued warming and constitute a potentially significant positive feedback to climate change. The highest consistent combustion levels are reported in interior Alaska and can be highly variable depending on the consumption of soil organic matter. Here we present an approach for quantifying emissions within a fire perimeter using remote sensing of fire severity. Combustion from belowground and aboveground pools was quantified at 22 sites (17 black spruce and five white spruce-aspen) within the 2010 Gilles Creek burn in interior Alaska, constrained by data from eight unburned sites. We applied allometric equations and estimates of consumption to calculate carbon losses from aboveground vegetation. The position of adventitious spruce roots within the soil column, together with estimated prefire bulk density and carbon concentrations, was used to quantify belowground combustion. The differenced Normalized Burn Ratio (dNBR) exhibited a clear but nonlinear relationship with combustion that differed by forest type. We used a multiple regression model based on transformed dNBR and deciduous fraction to scale carbon emissions to the fire perimeter, and a Monte Carlo framework to assess uncertainty. Because of low-severity and unburned patches, mean combustion across the fire perimeter (1.98 ± 0.34 kg C m^{-2}) was considerably less than within a defined core burn area (2.67 ± 0.40 kg C m^{-2}) and the mean at field sites (2.88 ± 0.23 kg C m^{-2}). These areas constitute a significant fraction of burn perimeters in Alaska but are generally not accounted for in regional-scale estimates. Although total combustion in black spruce was slightly lower than in white spruce-aspen forests, black spruce covered most of the fire perimeter (62%) and contributed the majority (67 ± 16%) of total emissions. Increases in spring albedo were found to be a viable alternative to dNBR for modeling emissions.

1. Introduction

Boreal forests store large amounts of organic carbon [*McGuire et al.*, 2009], particularly in soils, and are vulnerable to disturbance by wildfire. Annual fire occurrence in this biome is highly variable and tightly coupled to large-scale pressure systems controlling summer drought [*Hess et al.*, 2001; *Fauria and Johnson*, 2008; *Sedano and Randerson*, 2014]. Because fire weather conditions are projected to intensify during the 21st century, carbon emissions from boreal forest fires are increasingly recognized as an important positive feedback to climate change [*Flannigan et al.*, 2009; *National Research Council*, 2013].

Consistently, the highest levels of combustion (kg C m^{-2} burn area) in boreal forest fires are reported in interior Alaska [*French et al.*, 1996; *Kasischke et al.*, 2000; *Michalek et al.*, 2000; *Kasischke and Johnstone*, 2005; *Wirth*, 2005; *Kane et al.*, 2007; *Boby et al.*, 2010]. The majority of these occur in stands dominated by black spruce (*Picea mariana* (Mill.) BSP). Although black spruce trees are relatively small, they form dense stands that develop thick organic horizons insulated by moss and lichens. These forests are particularly prone to stand-replacing crown fires due to the amount, continuity, and moisture response time of their fuels [*Dyrness and Norum*, 1983; *Viereck*, 1983; *Ryan*, 2002]. Crown fires generate intense amounts of heat and can burn deep into the organic horizons of the forest floor [*Ryan*, 2002]. Interior Alaska has experienced a substantial increase in burn area during the last decade [*Kasischke et al.*, 2010] and is projected to burn more frequently and intensely throughout the 21st century [*Bachelet et al.*, 2005; *Balshi et al.*, 2009; *Euskirchen et al.*, 2009]. Carbon emissions from these fires, however, are variable and not well constrained at the regional level.

Carbon emissions are the product of burn area, fuel loads, carbon concentrations, and combustion efficiency (fraction of dry matter consumed). Most of the uncertainty surrounding fire emissions stems from a lack of knowledge on spatially explicit fuel loads and combustion efficiency [*French et al*., 2011]. Combustion efficiency in boreal forests is influenced by slope, aspect, vegetation cover, permafrost, drainage, weather, and the season of burn [*French et al*., 1996; *Kasischke et al*., 2000; *Kasischke and Johnstone*, 2005; *Kane et al*., 2007; *Shetler et al*., 2008; *Turetsky et al*., 2011]. Unlike burn area, however, these properties are difficult to observe at landscape and regional scales.

Field measurements are required to understand the magnitude of, and controls on, combustion. The majority of fire emissions in Alaska come from the forest floor [*Boby et al*., 2010]. In spruce forests, the position of adventitious roots in the soil column is relatively constant between trees and can be used to estimate prefire soil depth [*Kasischke and Johnstone*, 2005; *Boby et al*., 2010]. This assists calculations of soil combustion by improving accuracy and reducing the number of control sites needed. However, these measurements cannot be applied on a routine basis to monitor fires as they require a large number of laboratory analyses. As a proxy, the Composite Burn Index (CBI) [*Key and Benson*, 2005] has been developed for rapid assessment of fire severity. Fire severity is defined here by the immediate impacts of a fire on the landscape, including the destruction and combustion of live and dead carbon pools [*Lentile et al*., 2006; *Keeley*, 2009]. The CBI is based on visual characterizations of five forest strata, is used operationally as a rapid assessment of fire severity, and has been tested against a wide array of remotely sensed metrics [e.g., *van Wagtendonk et al*., 2004; *Epting et al*., 2005; *Miller and Thode*, 2007; *Allen and Sorbel*, 2008; *Hall et al*., 2008; *Hoy et al*., 2008; *Murphy et al*., 2008; *Soverel et al*., 2010; *Veraverbeke and Hook*, 2013]. However, the CBI also requires a large number of field measurements and its utility at estimating combustion and depth of burn in Alaska may be relatively limited because of its focus on aboveground vegetation [*Kasischke et al*., 2008; *Boby et al*., 2010].

A number of models have been developed to estimate emissions on regional scales, each with their benefits and limitations. Algorithms relating combustion to fire weather, such as the Canadian Forest Fire Behavior Prediction System [*Stocks et al*., 1989], have performed well in experimental fires but have demonstrated limited utility in wildland fires in Canada [*de Groot et al*., 2009] and Alaska [*Turetsky et al*., 2011]. Other operational models, such as CONSUME [*Ottmar et al*., 2006] and the First Order Fire Effects Model (FOFEM) [*Reinhardt et al*., 1997], require additional inputs of fuel type and moisture. As such they depend on the quality of these inputs, which are typically known to an uncertain degree across wildfire terrains. Larger-scale fire models require fewer data inputs but are spatially much coarser and do not consider region-specific factors. These models tend to estimate fuel loads as the balance between primary production, decomposition, and disturbance [e.g., *van der Werf et al*., 2010]. Other conceptual models have been derived from field data and expert knowledge on the major drivers, including topography, vegetation type, month of burn, and stand age [*Kasischke et al*., 1995, 2000, 2005; *French et al*., 2002; *Kasischke and Hoy*, 2012]. The above models have greatly improved our understanding and ability to generate plausible emissions scenarios. However, they can also provide combustion estimates with a surprisingly high range of variability [*French et al*., 2011].

None of the above approaches to modeling fire emissions utilize observations of fire severity, which may provide a critical constraint. Remote sensing, on the other hand, can provide spatially explicit information on fire severity over large areas. Because of its consistently high performance compared to other spectral indices [*Brewer et al*., 2005; *Epting et al*., 2005; *Hudak et al*., 2007; *Veraverbeke et al*., 2010a; *Veraverbeke and Hook*, 2013], the differenced Normalized Burn Ratio (dNBR) is the most commonly employed index. The dNBR quantifies fire severity from immediate (one season to 1 year) fire-induced changes in near- and shortwave infrared reflectance. Near-infrared reflectance typically decreases after fire due to the destruction of live vegetation and deposition of char, while shortwave infrared reflectance increases due to increased soil exposure and char, and water losses in the canopy and ground surface [*Chuvieco and Congalton*, 1988; *Eva and Lambin*, 1998; *Trigg and Flasse*, 2000; *Stroppiana et al*., 2002]. Thus, dNBR is generally sensitive to the removal of vegetation, charred surfaces, and soil exposure during nonwinter months in the boreal region [*Key and Benson*, 2005; *Lentile et al*., 2006; *Miller et al*., 2009].

As most trees are killed in the crown fires of Alaska, depth of burning in the forest floor is considered the most distinguishing feature of fire severity in the region [*French et al*., 2008]. Burn depth strongly regulates forest floor combustion efficiency and postfire forest succession [*Kasischke and Johnstone*, 2005; *Chapin et al*., 2006; *Turetsky et al*., 2011]. Because dNBR and similar indices are sensitive to canopy disturbance, their use as

indicators of fire severity in Alaskan boreal forests has been controversial. Some investigators have shown promising correlations between metrics of fire severity and dNBR [*Epting et al*., 2005; *Sorbel and Allen*, 2005; *Hudak et al*., 2007; *Allen and Sorbel*, 2008; *Hall et al*., 2008; *Verbyla and Lord*, 2008; *Soverel et al*., 2010], while others have found the opposite and argued against its utility [*Hoy et al*., 2008; *Murphy et al*., 2008]. Recently, *Barrett et al*. [2010, 2011] demonstrated that the inclusion of a large number of nonspectral and spectral inputs, including dNBR, can constrain depth-of-burn estimates across fire complexes. Ultimately, spectral indices will correlate with fire severity in most Alaskan fires only if burn depth is correlated with properties that influence the wavelengths considered.

Increases in spring albedo may serve as a useful severity metric in Alaska. While summer-based indices rely on differences in reflectance between live vegetation, charcoal, and mineral soil, spring albedo takes advantage of the variable snow exposure between burned and forested boreal landscapes. Increases in spring albedo are known to correlate with fire severity as reflective snow is exposed when trees are partially combusted and some fall to the ground [*Jin et al*., 2012].

Discrepancies in the performance of remote imagery for estimating ground-based properties of fire severity may come from the type and quality of field data, temporal and spatial characteristics of remote imagery, processing of remote sensing products, and/or unsatisfactory relationships between the metric of interest and spectral signatures. Here we investigate the performance of Landsat imagery for estimating carbon emissions within an individual fire event in interior Alaska and quantify the errors from influential sources. We combine remote sensing of fire severity (both dNBR and spring albedo) with direct measurements of belowground and aboveground combustion, accounting for within-site heterogeneity, distinct forest types, and available imagery. A regression model was used to scale site-level relationships between fire severity and combustion to the fire perimeter. We hypothesized that fire severity indices can be used to model carbon emissions for a single fire within a reasonable range of uncertainty, and that ground-based estimates of combustion may be higher than those for the entire perimeter due to unburned and low-severity patches.

2. Methods

2.1. Site Description

We investigated the Gilles Creek fire that burned approximately 8000 ha during 26 May to 2 June 2010 in interior Alaska (64°20′N; 145°45′W) (Figure 1). The dominant vegetation type within the burn perimeter was black spruce forest (62%, section 2.7), followed by mixed white spruce (*Picea glauca* (Moench) Voss)-aspen (*Populus tremuloides* Michx) forests (17%), and pure aspen (5%). Birch (*Betula nana* L.) and willow (*Salix* spp. L.) shrub stands were found in southern areas of the perimeter (13% of the fire scar), although these were mostly left unburned. The terrain consisted primarily of gently sloping south facing uplands on Inceptisols. Mean slope (calculated from a 35 m digital elevation model, discussed in section 2.6) at the study sites was 2.4°, although terrain was steeper in the far north of the perimeter reaching maximum values of 31°. Permafrost is discontinuous in the region and was not present at our burned or control sites. Long-term (1950–2000) mean annual temperature was −3°C, and mean annual precipitation was 312 mm [*Hijmans et al*., 2005].

2.2. Field Surveys

We selected 22 burned sites within the fire perimeter and eight control sites in close proximity (Figure 1 and Table 1). Field sites were located between 120 and 700 m away from an access road traversing the center of the fire. We chose burned sites within a wide range of fire severity, derived from visual assessment and a dNBR layer from the Monitoring Trends in Burn Severity (MTBS) database [*Eidenshink et al*., 2007]. In order to minimize positional errors between field sites and remote imagery, we attempted to choose sites within relatively homogenous 100 m× 100 m patches of vegetation and fire severity. Sites were selected from the two dominant prefire vegetation types: 17 were in black spruce and five in white spruce-aspen forests (together comprising 79% of the burn perimeter and 86% of the core burn area, section 2.7). Control sites were selected to match conditions at the burned plots: three control sites contained black spruce with sphagnum moss (C01, C02, and C03), two contained black spruce with feather mosses and lichens (C07 and C08), and three contained mixed white spruce-aspen stands (C03, C04, and C08) (Table 1). Centroid coordinates for each site were recorded with a handheld GPS system (GeoExplorer 6000 series GeoXH GPS device, Trimble, Sunnyvale, CA; 1 m error in *x* and *y*).

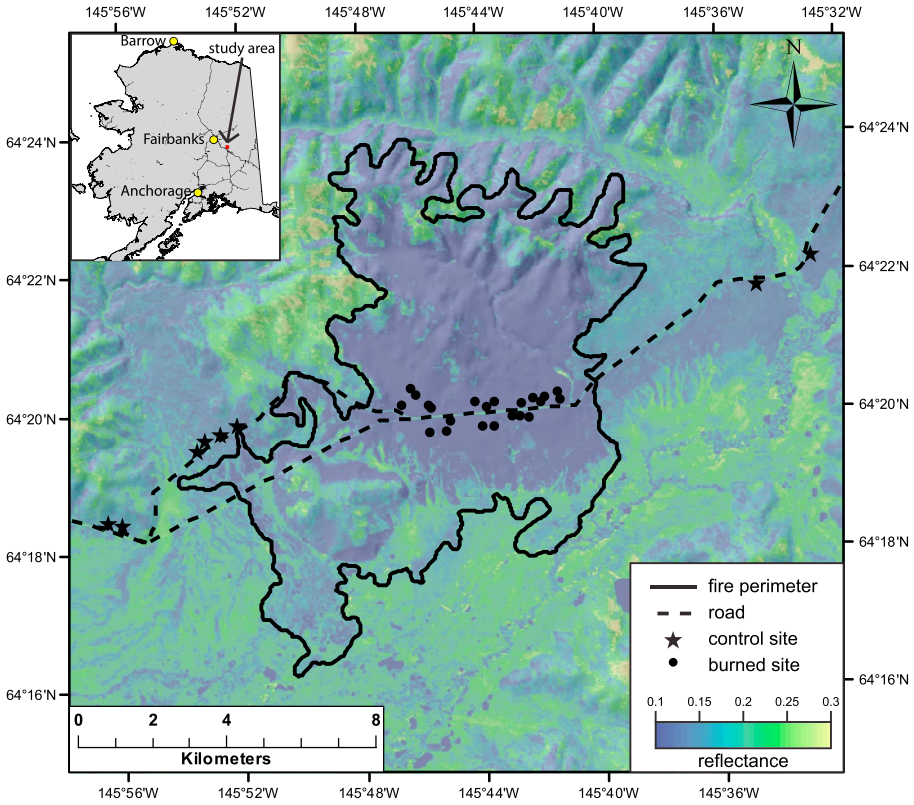

Figure 1. Map of the Gilles Creek fire in interior Alaska. The background image is surface reflectance from a Landsat Thematic Mapper band 4 (0.76–0.90 μm) postfire image (Landsat 5, row 15, path 67, 15 August 2010). The hillshade effect was generated from a 35 m digital elevation model [*Mamini et al*., 2008] to show steeper terrain in the north.

Field surveys were conducted between 27 and 31 August 2012. We established a 2 m × 30 m transect in the north–south direction within each site. Six soil cores were taken within each transect and selected semirandomly to represent the range of forest floor conditions. Because some soil properties may differ by the proximity of trees [*Boby et al*., 2010], three cores were chosen next to trees (as close as possible, typically 3–10 cm) and three further away (mean of 98 cm). A soil corer with 4.8 cm diameter (5/8″ threading soil core sampler, Arts Machine Shop, American Falls, ID, USA) was used to extract organic soil samples. According to the classification of *Manies et al*. [2004], we separated the soil organic horizons into moss (live and dead), fibric (mildly decomposed material with roots and recognizable moss parts), mesic (moderately decomposed with few recognizable plant parts), and humic (highly decomposed organic matter at the interface with mineral soil). Horizons were separated with a knife, and their lengths were measured. It should be noted that we extracted humic horizons at the interface of mineral soil. Some of these samples included topsoil mineral horizons, contributing to relatively high bulk densities and low carbon concentrations (Figure 2).

We recorded distances between the surface and the top of the mineral soil and, for cores next to spruce trees, between the surface and the highest adventitious root. In our sites, black and white spruce trees typically formed adventitious roots. These fine roots are grown in the upper soil horizons in response to unfavorable temperature and moisture conditions deeper in the soil column [*Lebarron*, 1945]. Their position in the soil column has proven useful for estimating prefire soil depths [*Kasischke and Johnstone*, 2005; *Kasischke et al*., 2008; *Boby et al*., 2010].

Species, diameter at breast height (DBH), and the position of the highest adventitious root within the soil column, if present, were recorded for every tree inside each transect, regardless of size. At burned sites we visually estimated the fractional consumption of cones, needles, fine and coarse branches, and bark. To assess its relationship with emissions and satellite indices, we also calculated the Composite Burn Index (CBI) [*Key and Benson*, 2005], modified for the shorter stand structures in interior Alaska by *Kasischke et al*. [2008].

Table 1. Overview of the Burned and Control Sites in or Near the Gilles Creek Fire

Site	Latitude (North)	Longitude (West)	Forest Type[a]	dNBR[b]	Belowground Carbon/Combustion[c,d] (kg C m^{-2})	Aboveground Carbon/Combustion[c,e] (kg C m^{-2})	Total Carbon/Combustion[c,f] (kg C m^{-2})
				Control			
C01	64.3308	145.8703	BS	0.099	3.60	1.84	5.44
C02	64.3289	145.8797	BS	0.102	3.26	1.15	4.41
C03	64.3071	145.9348	WSA	0.123	1.81	1.57	3.37
C04	64.3078	145.9426	WSA	0.134	3.00	2.04	5.03
C05[g]	64.3248	145.8930	BS	0.062	12.45	0.57	13.02
C06	64.3630	145.5787	BS	0.078	4.45	0.79	5.25
C07	64.3699	145.5485	BS	0.089	3.21	2.35	5.55
C08[h]	64.3272	145.8880	WSA	0.098	3.33	1.49	4.83
				Burned			
B01	64.3361	145.6895	BS	1.039	4.14 (2.85)	1.69 (1.57)	5.83 (4.41 ± 0.54)
B02	64.3355	145.7005	WSA	0.649	3.31 (2.22)	1.63 (0.80)	4.93 (3.02 ± 0.21)
B03	64.3391	145.7729	BS	1.005	5.16 (1.82)	0.77 (0.67)	5.93 (2.49 ± 0.54)
B04	64.3376	145.7697	BS	0.737	4.58 (1.12)	1.14 (0.47)	5.72 (1.60 ± 0.76)
B05	64.3352	145.7780	BS	1.052	3.88 (2.22)	0.57 (0.49)	4.45 (2.71 ± 0.38)
B06	64.3379	145.6912	BS	1.006	3.69 (2.13)	0.90 (0.77)	4.60 (2.90 ± 0.39)
B07	64.3367	145.6981	WSA	0.852	3.61 (2.33)	1.87 (1.02)	5.47 (3.34 ± 0.29)
B08	64.3363	145.7046	BS	0.957	3.06 (1.68)	0.82 (0.59)	3.89 (2.28 ± 0.20)
B09	64.3357	145.7263	BS	1.044	4.14 (2.51)	1.20 (0.84)	5.34 (3.35 ± 0.31)
B10	64.3345	145.7304	BS	0.978	4.29 (2.10)	1.79 (1.25)	6.08 (3.35 ± 0.40)
B11	64.3358	145.7373	BS	1.100	4.94 (3.18)	1.24 (0.93)	6.18 (4.11 ± 0.42)
B12	64.3299	145.7329	BS	1.064	4.80 (2.75)	0.95 (0.74)	5.74 (3.48 ± 0.28)
B13	64.3296	145.7274	WSA	0.674	3.47 (2.55)	2.82 (1.64)	6.29 (4.19 ± 0.37)
B14	64.3344	145.7616	BS	0.717	4.12 (1.59)	1.42 (0.40)	5.54 (1.99 ± 0.37)
B15	64.3340	145.7632	BS	0.543	4.13 (0.85)	1.19 (0.15)	5.32 (1.00 ± 0.38)
B16	64.3311	145.7511	BS	1.013	3.26 (1.87)	1.06 (0.80)	4.31 (2.68 ± 0.38)
B17	64.3289	145.7531	BS	0.969	4.01 (1.32)	1.40 (1.01)	5.40 (2.34 ± 0.31)
B18	64.3285	145.7625	WSA	0.553	4.36 (1.79)	1.68 (0.46)	6.04 (2.25 ± 0.44)
B19	64.3321	145.7160	BS	1.032	3.34 (1.90)	1.24 (0.96)	4.58 (2.86 ± 0.38)
B20	64.3321	145.7117	BS	0.955	2.24 (1.42)	1.23 (0.81)	3.48 (2.24 ± 0.21)
B21	64.3317	145.7073	WSA	0.707	3.37 (3.00)	3.75 (0.62)	7.12 (3.62 ± 0.39)
B22	64.3353	145.7112	BS	0.991	3.14 (2.17)	1.42 (1.09)	4.56 (3.26 ± 0.41)

[a] BS = black spruce; WSA = white spruce-aspen.
[b] Differenced Normalized Burn Ratio.
[c] Estimated prefire carbon. Values in parentheses represent combustion.
[d] Belowground carbon in burned sites represents the average of estimated prefire carbon in each soil core. Combustion was adjusted for the depth of burn at every tree in a transect.
[e] Aboveground carbon is estimated prefire carbon from assumed combustible pools (cones, needles, branches, bark).
[f] Uncertainty estimates for total combustion derived from Monte Carlo simulations.
[g] Because of the deep organic soil at this site, only its carbon concentration and bulk density properties were used for calculations.
[h] Chosen to match conditions at a moist white spruce-aspen burned site with more developed soil horizons (B18) and used only for calculations of this site's prefire soil properties.

2.3. Laboratory Analysis

A total of 424 soil samples were dried, weighed, homogenized, and analyzed for carbon concentrations (not all cores contained all four soil horizons). As in *Kasischke et al.* [2000] and *Boby et al.* [2010], soils were dried to constant weight at 65°C (for 6 days). Particles greater than 2 mm in diameter, including branches, roots, and gravel, were removed from samples, and their weights and volumes subtracted from the calculation of bulk densities. Samples were homogenized with a Wiley mill and 40 mm sieve. We used an element analyzer (FlashEA 1112, Thermo Fisher Scientific, Waltham, MA, USA) to determine the carbon concentration by mass for every sample.

2.4. Belowground Combustion

We quantified soil combustion in each burned site similar to *Boby et al.* [2010]. Measurements of adventitious root positions within the soil column were used in conjunction with bulk density and carbon concentrations to calculate prefire soil carbon stocks. Combustion was calculated as the difference between these and measured postfire soil carbon stocks.

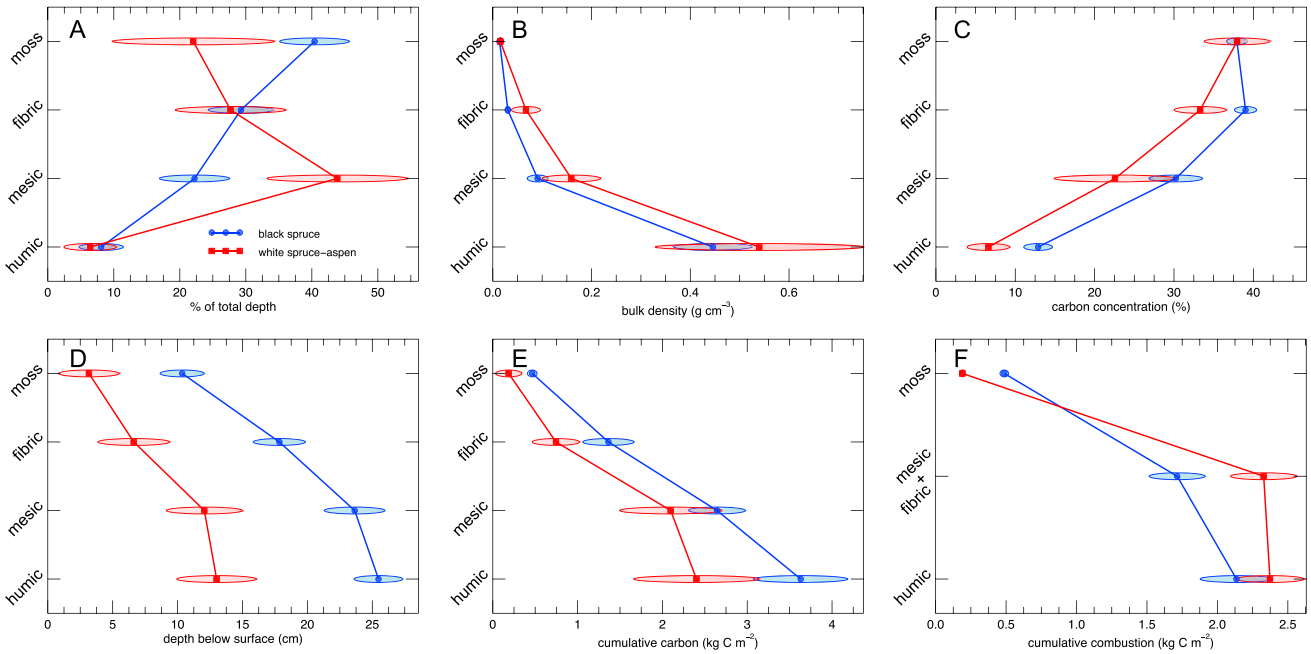

Figure 2. Soil characteristics by horizon, separated by black spruce and white spruce-aspen forests: (a) percent of total soil organic column depth, (b) bulk density, (c) carbon concentration, (d) depth of horizon's bottom interface below the surface floor, (e) cumulative carbon, and (f) cumulative combustion. Figures 2a–2e are derived from control sites, and relationships in Figures 2a–2e were used in the reconstruction of burned core prefire carbon stocks (Table S1). Oval widths represent 95% confidence intervals.

Because of fundamental differences in soil properties, black spruce and white spruce-aspen sites were treated individually in our calculations of belowground combustion. Organic horizons in black spruce control sites were roughly twice as deep as those in white spruce-aspen, with more developed moss horizons, higher carbon concentrations, and lower bulk densities (Figure 2). As a result, these soils stored 51% more carbon on average (mean of 3.63 kg C m^{-2} for black spruce versus 2.40 kg C m^{-2} for white spruce-aspen).

We first estimated prefire depths for each soil horizon in burned sites (Table S1 in the supporting information) assuming that horizons had undergone some degree of pyrolysis that resulted in reduced carbon storage. Soil horizons tended to become somewhat compacted during the process of core extraction: mean compaction was 10% for burned and 58% for control sites. To account for this in bulk density calculations, we used measurements of total column depth as a baseline and assumed soil horizons were compacted to a degree proportional to their proximity to the soil surface. The relationship between total depth and distance between adventitious roots and the mineral soil was strongly linear using all control sites ($r^2 = 0.86$, $p < 0.001$, Table S1). Prefire soil depths for burned cores close to trees were estimated using this relationship. Total depths for cores away from trees were taken as the mean of those close to trees in a given site.

Individual soil horizon depths were observed to be a relatively constant fraction of total distance to mineral soil in control sites, with the exception of humic ($p < 0.01$ for slopes of moss, fibric, and mesic horizons versus total depth in both forest types). We therefore used these ratios in conjunction with total depths to assign prefire horizon depths to burned soil cores (Figure 2). Because the humic horizon was absent in some control sites (29% of cores in black spruce and 50% in white spruce-aspen sites), we did not assign a prefire humic horizon to burned soil cores that also lacked one. If a burned core did have a humic horizon (the predominant case), the depth of its prefire humic horizon was taken as the mean from control sites. In each case the remaining horizon fractions were adjusted accordingly (Table S1).

Prefire horizon depths were multiplied by prefire bulk densities and carbon concentrations to determine prefire soil carbon stocks. Prefire bulk densities and carbon concentrations varied by horizon and forest type (Figure 2 and Table S1). These properties were derived from control cores as burning significantly altered their values: in general, bulk density was higher and carbon concentration was lower in the mesic and fibric horizons of burned sites versus control ($p < 0.001$ in all cases). Because bulk densities, carbon concentrations,

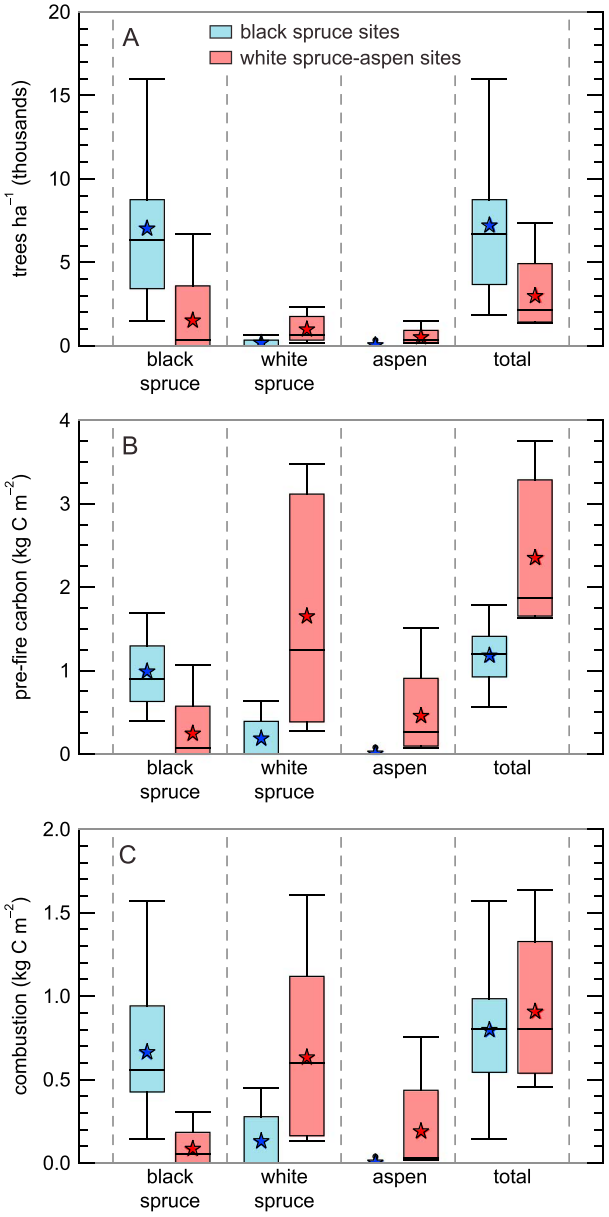

Figure 3. Box plots of burned site aboveground (a) tree density, (b) prefire carbon, and (c) combustion, separated by species and assigned forest type. Populations were drawn from site-level means. Prefire carbon in Figure 3b and combustion in Figure 3c are from the assumed combustible pools (cones, needles/leaves, fine and coarse branches, and bark). Stars represent overall means by species. Note that sites categorized as black spruce contained some white spruce trees, and sites categorized as white spruce-aspen contained some black spruce trees, although these contributed little to total carbon pools or emissions.

and horizon depths were not found to differ significantly by the proximity of cores to trees ($p > 0.05$), we did not factor this into our calculations. In all cases, soil properties for black spruce and white spruce-aspen sites were considered separately whenever control values were significantly different (Table S1).

Postfire carbon stocks were calculated independently for each soil horizon as the product of its mass and carbon concentration. Combustion was calculated as the difference between prefire and postfire stocks, not allowing negative values. Because of the relative difficulty in consistently separating fibric and mesic horizons, these were pooled for combustion calculations.

Burned plots displayed a high degree of variability in the consumption of duff (fibric, mesic, and humic horizons). To better account for this, we utilized measurements of adventitious root positions for every tree in burned transects. Using mean values for the distance between adventitious roots and the top of the moss horizon derived from control sites (5.9 cm for black spruce and 5.3 cm for white spruce-aspen sites), depth of burn was found to strongly relate to soil combustion ($r^2 = 0.73$ for an exponential fit with black spruce and $r^2 = 0.73$ for a linear fit with white spruce-aspen cores) (Figure S1). We applied these relationships, separate for each forest type, to the depth of burn at every tree. The final value for mean soil combustion at a given site was taken as the average of (1) mean combustion from its six soil cores and (2) combustion calculated from the depth of burn at every tree.

2.5. Aboveground Combustion

We used a number of DBH-based allometric equations to estimate prefire carbon for the foliage, cones, fine and coarse branches and bark of all trees in the burned sites (Figures 3 and 4). As in *Boby et al.* [2010], we assumed that emissions from boles and roots were zero because of their typically low levels of consumption [*Campbell et al.*, 2007]. Equations from interior Alaska and Canada were used for black spruce [*Barney et al.*, 1978; *Mack et al.*, 2008; *Ung et al.*, 2008; *Boby et al.*, 2010], white spruce [*Yarie and Vancleve*, 1983; *Ung et al.*, 2008], and aspen [*Mack et al.*, 2008; *Ung et al.*, 2008]. In each case the mean value from the collection of allometric equations was used. Using a mean chemical composition of woody plants [*Randerson et al.*, 2006b], we assigned tree carbon pools a carbon concentration of 0.45. To calculate plot-level combustion of

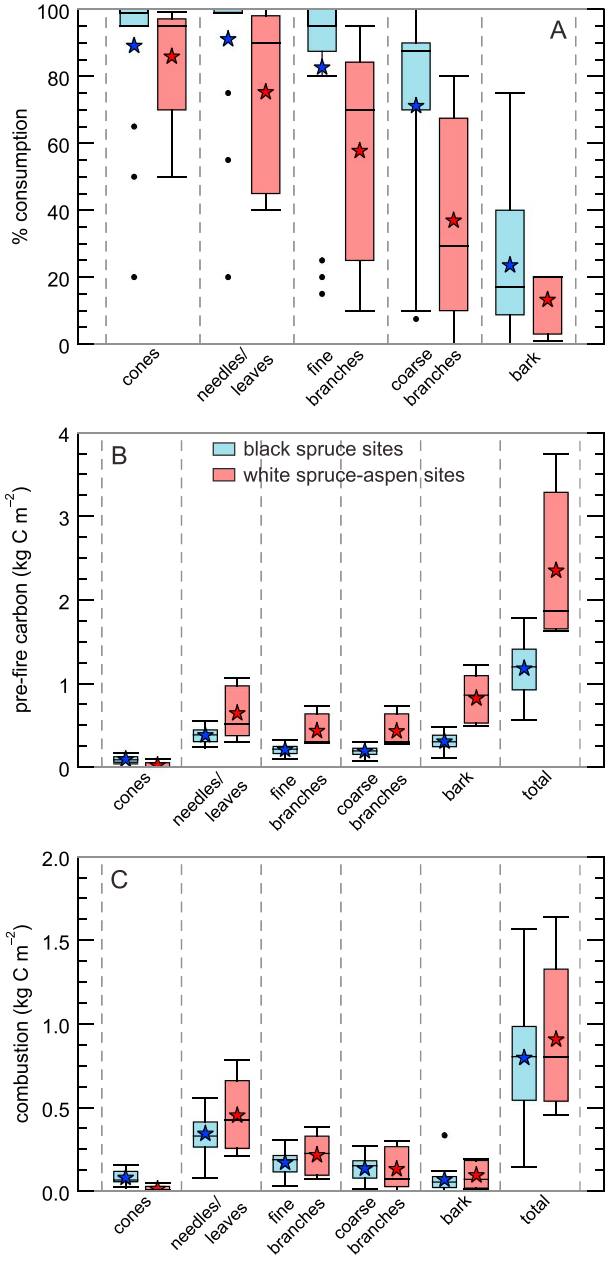

Figure 4. Box plots of burned site aboveground (a) percent consumption, (b) prefire carbon, and (c) combustion, separated by assumed combustible carbon pool and forest type. Populations were drawn from site-level means. Values less than the 25th percentile or greater than the 75th percentile are depicted as dots. Stars represent overall means by carbon pool.

aboveground vegetation, estimates of percent consumption were multiplied by the prefire carbon for each pool and averaged over each transect.

2.6. Remote Sensing of Fire Severity

The dNBR from Landsat Thematic Mapper (TM) and Enhanced Thematic Mapper Plus (ETM+) imagery was used to characterize fire severity and to scale plot-level carbon emissions to the fire perimeter. Landsat imagery was chosen because of its comparatively fine scale (30 m for dNBR bands) and moderate revisit time (16 days). Because of potential cloud contamination and data gaps, we elected to use all available summer images (1 July to 31 September). We downloaded 11 Level 1 georectified images from 2009 and 11 from 2010 from the U.S. Geological Survey (USGS) Global Visualization Viewer website [*U.S. Geological Survey*, 2012] (Table S2). We used the Landsat Ecosystem Disturbance Adaptive Processing System (LEDAPS) to calculate surface reflectance [*Masek et al.*, 2006]. LEDAPS converts digital numbers, calibrates at-sensor radiance values, and corrects for atmospheric contamination using column water vapor from National Centers for Environmental Prediction reanalysis and ozone concentration from Total Ozone Mapping Spectrometer data aboard the Nimbus 7, Meteor 3, and Earth Probe platforms.

Roads, water bodies, and clouds were masked out for every image. To ensure no contamination of vegetation reflectance, a 90 m buffer was applied to roads. A 60 m buffer was applied to water bodies, which were determined from visual inspection of visible and near-infrared bands and comparison with the Landscape Fire and Resource Management Planning Tools (LANDFIRE) vegetation map [*U.S. Department of Interior, Geologic Survey*, 2009]. While LEDAPS generates a cloud mask based on the Automatic Cloud Cover Assessment algorithm [*Irish et al.*, 2006], we determined coverage to be incomplete for many clouds and their shadows. We therefore manually masked out clouds and cloud shadows using all available bands. We adopted a modified version of the rotation method [*Tan et al.*, 2010] to correct for topographic influences on reflectance. This procedure normalizes reflectance by flattening the linear relationship between surface reflectance and cosine of the incidence angle (Figure S2). Slope and aspect were calculated in ArcGIS 10.1 from a 35 m digital elevation model [*Mamini et al.*, 2008] to determine incidence angles, resampled to 30 m Landsat resolution using

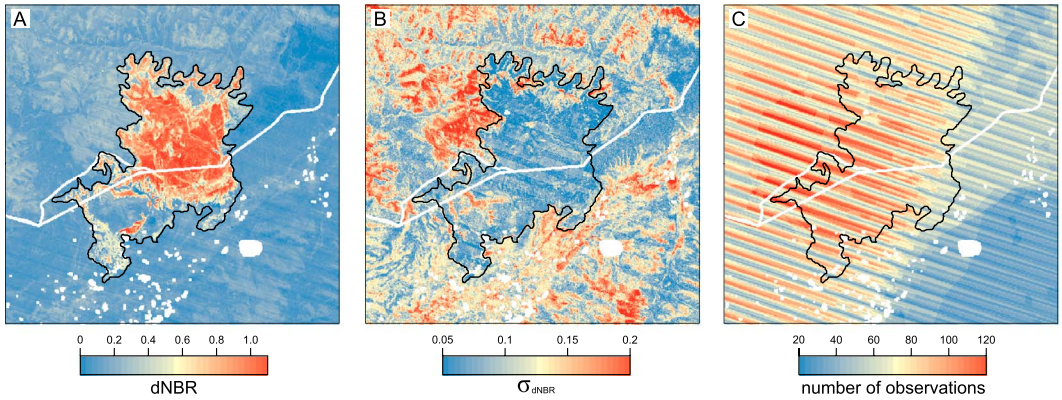

Figure 5. (a) Mean dNBR, (b) standard deviation of dNBR, and (c) number of dNBR observations for each pixel. Variability in dNBR was highest for deciduous vegetation outside the burn area. The number of observations was reduced from a maximum of 121 (11 prefire and 11 postfire images) due to incomplete coverage in one of three tiles (row 15, path 69), clouds, and data gaps in Landsat 7 imagery (seen as stripes in Figure 5c).

bilinear interpolation for slope and nearest neighbor for aspect. Because images were often collected on different days of the year, we applied a correction factor similar to that presented in *Veraverbeke et al*. [2010b]. This acted to adjust the mean reflectance for a given image to its predicted mean reflectance at an angle of 64.9° (equal to noon on the area's summer solstice). We performed the method separately for pixels inside and outside the core burn area (defined in section 2.7). While this method accounts for the dependence of surface reflectance on slope, aspect, and timing of satellite overpass, it does not correct for seasonal influences on spectral signatures caused by vegetation phenology.

Normalized Burn Ratio (NBR) was calculated for each scene according to

$$\mathrm{NBR} = \frac{\rho_4 - \rho_7}{\rho_4 + \rho_7} \tag{1}$$

where ρ_4 = band 4 reflectance (0.76–0.90 μm) and ρ_7 = band 7 reflectance (2.08–2.35 μm). The dNBR for every prefire–postfire scene combination was defined by

$$\mathrm{dNBR} = \mathrm{NBR}_{\mathrm{prefire}} - \mathrm{NBR}_{\mathrm{postfire}}. \tag{2}$$

Because of clouds, missing areas in the row 15 path 69 tile, and "stripes" of data gaps from a failed Scan Line Corrector in Landsat 7 images, the number of scene combinations differed by pixel. Our final dNBR map used to model carbon emissions was derived from the mean of all possible prefire and postfire scene combinations in each pixel (Figure 5).

As an alternative approach, we used fire-induced increases in spring albedo as a metric for fire severity. We downloaded five scenes between 22 February and 10 April from 2009 and four from 2012 (Table S2). Images were processed and terrain corrected as above, but incidence angles were normalized to noon on the vernal equinox (41.5°). Broadband albedo was quantified using narrowband-to-broadband conversion algorithms from *Liang* [2001].

2.7. Modeling Carbon Emissions

We constructed a model of combustion based on dNBR at our field sites. dNBR was extracted from the pixel containing the centroid of each field site. As has been shown for other fire severity metrics [*Epting et al*., 2005; *Allen and Sorbel*, 2008; *Verbyla and Lord*, 2008], the relationship between dNBR and combustion varied by forest type (Figure 6). Whereas black and white spruce are difficult to separate spectrally, deciduous broadleaf vegetation exhibits a unique spectral signature compared to conifers [*Nelson et al*., 1984; *Shen et al*., 1985; *DeFries et al*., 1995]. To account for this and apply the model to the entire fire scar, we derived a fractional deciduous layer from spectral mixture analysis. Because of the high tree densities, we used a simplified two-end-member model (deciduous and conifer trees) and assumed that the fractional cover of other spectral features (e.g., soils and shadows) were of minimal importance. Two end-member polygons were selected

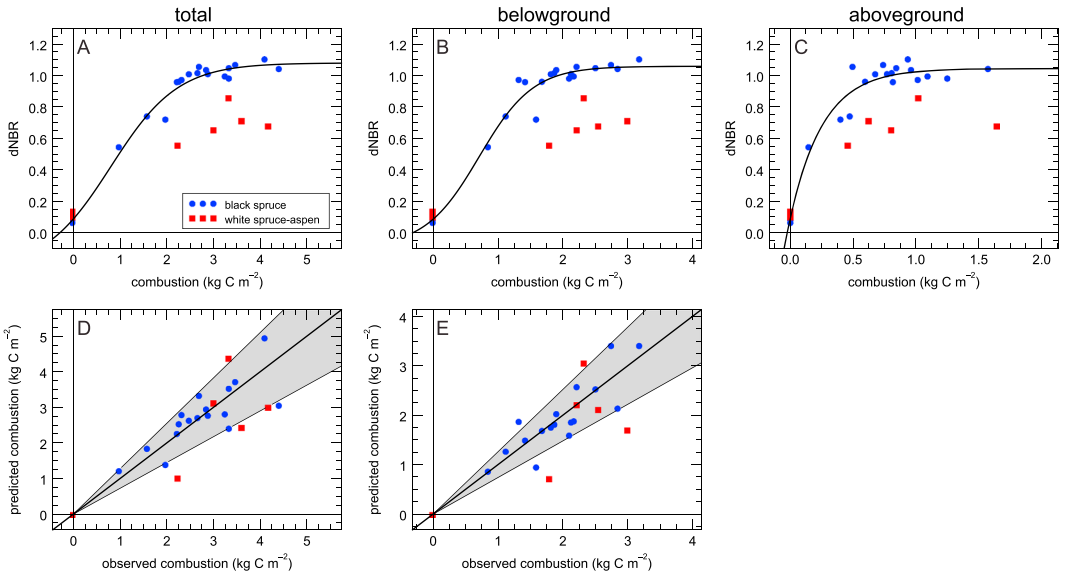

Figure 6. Relationships between dNBR and (a) total, (b) belowground, and (c) aboveground combustion for each forest type. Lines in Figures 6a–6c represent logistic fits for black spruce. A multiple linear regression with inputs of logistic-transformed dNBR and deciduous fraction × dNBR was used to model (d) total and (e) belowground combustion. Shaded areas represent one standard error for estimated prediction errors.

from areas of known black spruce and aspen dominance (Figure 7). We performed a constrained linear spectral unmixing using inputs of Landsat TM and ETM+ bands 1 (0.45–0.52 μm), 2 (0.52–0.60 μm), 3 (0.63–0.99 μm), 4 (0.76–0.90 μm), 5 (1.55–1.75 μm), and 7 (2.08–2.35 μm) from a complete prefire image (Landsat 5, 3 August 2009, row 15, path 68). The outputs of this unmixing model were fraction of deciduous and conifer cover, which sum to one for each pixel.

To model combustion we normalized dNBR values by the mean at control sites. Because it varied nonlinearly with combustion, dNBR was transformed according to a logistic fit using all black spruce sites (Figure 6). We then fit a multiple linear regression (MLR) using all sites with two terms: (1) transformed dNBR and (2) the product of dNBR and deciduous fraction. The latter term had the effect of accounting for the disparate relationship between dNBR and combustion in white spruce-aspen stands without artificially inflating unburned and low-severity sites. We held the constant term at zero. The influence of the second term was constrained by maximum values of dNBR (0.85) and deciduous fraction (0.25). These thresholds were implemented to avoid unnecessary inflation of combustion in pixels with high deciduous fractions and dNBR, and their values represent the approximate maximum values observed at our field sites. Any points with original dNBR values less than the maximum dNBR at control sites (0.134) were fixed at zero combustion. Predicted combustion was also constrained by a minimum of zero and maximum of 1.2 times the maximum

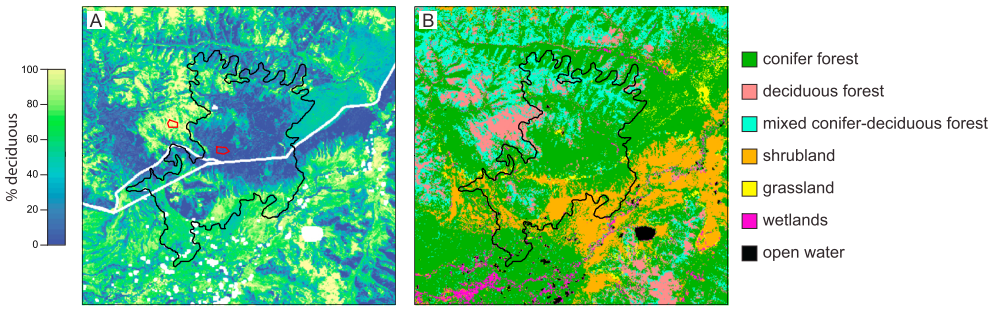

Figure 7. Maps of (a) deciduous fraction and (b) vegetation type. Deciduous fraction was derived from a linear spectral unmixing model using end-member polygons from known deciduous and conifer stands (shown in red). Vegetation types in Figure 7b were aggregated from the LANDFIRE data set [*U.S. Department of Interior, Geologic Survey*, 2009].

observed combustion from our burned sites. The maximum threshold was implemented because of the steep slope at high dNBR values but was reached in only 0.4% of pixels. As an alternative we modeled emissions using increases in spring albedo. All methodology was the same as above, except that the influence of deciduous vegetation on emissions (second MLR term) was constrained by a spring albedo increase of 0.2 as opposed to a dNBR threshold of 0.85.

We applied the resulting model across the entire fire perimeter, which was taken from the MTBS database. To account for unburned islands within the fire perimeter, we defined a "core burn area" for some analyses. This was designated by a minimum dNBR threshold of 0.2 within the burn perimeter using Landsat 5 images from 3 August 2009 (row 15, path 68) and 15 August 2010 (row 15, path 67). The core burn area covered 70% of the fire scar. We used an aggregated version of the LANDFIRE vegetation map to analyze patterns for each forest type across the perimeter (Figure 7). Although land cover types did not correspond exactly at our field sites, 63% of our white spruce-aspen sites were adjoined by at least one mixed white spruce-hardwood forest pixel from LANDFIRE, opposed to only 18% of our black spruce sites.

2.8. Uncertainty Analysis

We adopted a Monte Carlo framework to characterize uncertainty in our modeled carbon emissions. Uncertainties were assumed to come from three major categories of sources: belowground combustion, aboveground combustion, and landscape scaling. A total of 1000 simulations were performed where inputs varied by either the distribution of influential parameters or methodological choices (details given in Table S3). For each major category, we identified the most prominent sources of error associated with our approach. We identified six sources for belowground combustion. These related to instrument error, assumptions about prefire bulk density, carbon concentrations, and humic horizons, calculations of soil carbon losses, soil core selection, and site-level scaling for duff consumption. The three main sources we identified for aboveground combustion were carbon concentration of tree biomass, biases in the visual estimates of consumption, and choice of allometric equation.

Landscape scaling was associated with six uncertainty sources: image acquisition date range, number of Landsat images used, assumptions about the maximum level of combustion for any given pixel, positional errors, regression prediction error, and the distribution of forest types across the fire perimeter. Positional errors can be introduced from a number of sources, including geometric calibration, image-to-image registration, and field site coordinates. We addressed this uncertainty in our extraction of dNBR and deciduous fraction with several spatial averaging techniques (Table S3). Prediction error is typically associated with two sources: estimation of the mean and variance of the residuals. We focused on residual variance because the mean prediction varied with all other uncertainty sources. Because of the nonlinear relationship between dNBR and combustion, residual error tended to increase with combustion (Figure 6). We therefore characterized an uncertainty range that varied linearly between the standard residual error of the first and last eight points, ordered by observed combustion. This had the property that 68% of burned points were within one standard error, matching an expected normal distribution.

Because fire-wide means in these simulations were slightly different (12% higher) than those in our main approach, all uncertainty estimates were normalized by the ratio of means for each reported metric. This assumes a constant coefficient of variation. We also performed a series of simulations to quantify the individual contributions from each category of uncertainty (belowground, aboveground, and landscape scaling). In each case two scenarios were implemented: one where the source category was removed by holding its values and/or methods constant and one where it was the only contributing factor. Uncertainties in emission estimates modeled with spring albedo were derived in a similar manner, except we did not vary the acquisition date range because of fewer available images.

3. Results

3.1. Site-Level Combustion

Depth of burn ranged between 0.8 and 30.3 cm, with a mean of 19.2 cm at black spruce, 11.5 cm at white spruce-aspen, and 17.5 cm across all burned soil cores (Figure S1). This corresponded to a range of soil core combustion between 0.12 and 5.14 kg C m^{-2}, with a mean of 2.14 kg C m^{-2} at black spruce, 2.37 kg C m^{-2} at white spruce-aspen, and 2.19 kg C m^{-2} across all cores. When scaled by the depth of burn at all sampled

Table 2. Carbon Emissions at the Site and Landscape Levels

	Sites[a]	Core Burn Area[b]	Fire Scar[b]
Total emissions (Gg C)	NA	149 ± 22	158 ± 27
Black spruce	NA	102 ± 15	105 ± 17
White spruce-aspen	NA	27 ± 4	30 ± 5
Combustion (kg C m^{-2})	2.88 ± 0.23	2.67 ± 0.40	1.98 ± 0.34
Black spruce	2.77 ± 0.26	2.65 ± 0.40	2.12 ± 0.34
White spruce-aspen	3.28 ± 0.24	2.94 ± 0.41	2.19 ± 0.38
Fraction of emissions (%)			
From black spruce	NA	68.5 ± 16.2	66.6 ± 17.0
From white spruce-aspen	NA	18.2 ± 4.4	18.8 ± 4.4
From belowground[c]	71.5 ± 5.2	69.3 ± 4.9	68.9 ± 4.9
From aboveground[c]	28.5 ± 5.2	30.7 ± 4.9	31.2 ± 4.9

[a]Uncertainties estimates are given as standard errors taken from Monte Carlo simulations of aboveground and belowground combustion. NA = not applicable for site-level estimates.
[b]Uncertainty estimates are given as standard errors for fire-wide means. Uncertainty at any given pixel was typically higher.
[c]For site-level values, defined as the mean contribution to total combustion. For landscape levels, defined as the contribution to total fire-wide emissions.

trees, mean belowground combustion was 2.06 kg C m^{-2} across all sites (Table 1). Soil horizons in black spruce forests tended to be deeper and had higher carbon concentrations. However, these soils were also moister and less dense (Figure 2). As a result they stored more carbon but experienced less fractional consumption: mean consumption of soil organic matter was 53% at black spruce sites and 66% at white spruce-aspen. Except in the lowest severity sites, moss horizons were completely consumed (mean of 95%) but contributed to only 19% of belowground combustion. Fibric and mesic horizons together experienced 54% consumption on average and contributed to the majority (65%) of soil combustion. Only 37% of carbon in humic horizons was consumed, contributing to 15% of total soil combustion (Figure 2).

Black spruce formed dense stands (7010 trees ha^{-1} in burned black spruce sites, Figure 3), but these trees were relatively small: 2.93 kg C $tree^{-1}$ total aboveground and 1.20 kg C $tree^{-1}$ in assumed combustible pools (cones, needles, branches, and bark). White spruce trees that occurred in our black spruce sites were larger (11.10 kg C $tree^{-1}$ in combustible pools) but contributed to only 16% of the 1.18 kg C m^{-2} in total prefire combustible carbon (Figure 3). Although white spruce-aspen sites contained some black spruce, the majority of the 2.35 kg C m^{-2} in combustible biomass came from relatively large white spruce (17.07 kg C $tree^{-1}$ combustible) and aspen (9.77 kg C $tree^{-1}$ combustible) trees (Figure 3).

Mean consumption was highest for cones (89% in black spruce and 86% in white spruce-aspen sites) and needles/leaves (91% in black spruce and 75% in white spruce-aspen), followed by fine branches (83% in black spruce and 58% in white spruce-aspen), coarse branches (71% in black spruce and 37% in white spruce-aspen), and bark (24% in black spruce and 13% in white spruce-aspen) (Figure 4). Although combustible biomass in white spruce-aspen sites was over twice that in black spruce, mean aboveground combustion was similar due to less fractional consumption (0.80 kg C m^{-2} in black spruce versus 0.91 kg C m^{-2} in white spruce-aspen, Figure 4).

Total site-level combustion ranged between 0.99 and 4.41 kg C m^{-2}, with a mean of 2.77 kg C m^{-2} in black spruce, 3.28 kg C m^{-2} in white spruce-aspen, and 2.88 kg C m^{-2} overall (Tables 1 and 2). Seventy-two percent of combustion was from the soil. Belowground and aboveground combustion were positively correlated: $r = 0.57$ for black spruce and 0.51 for all sites (Figure S3).

3.2. Remote Sensing of Fire Severity

The total number of dNBR values for a given pixel varied between 18 and 121 across the domain and between 25 and 121 within the fire scar. Mean dNBR was 0.75 in the core burn area, 0.57 across the entire fire scar, and 0.14 outside the fire scar (Figures 5 and S4). dNBR ranged between 0.54 and 1.10 at the burned sites, with a mean of 0.95 at black spruce, 0.69 at white spruce-aspen, and 0.89 overall (Figure 6). Control sites exhibited an average dNBR of 0.10. Variability in dNBR was driven in part by vegetation phenology and therefore more constant in burned areas (Figure 5): the standard deviation of dNBR averaged 0.07 within the

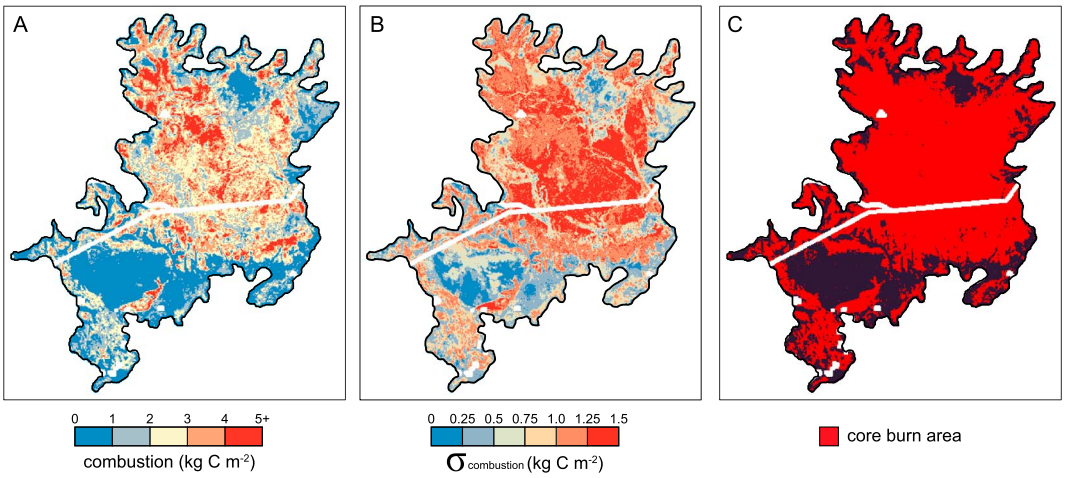

Figure 8. Maps of (a) mean and (b) standard error of modeled combustion within the Gilles Creek fire perimeter. Variance in Figure 8b was derived from 5000 Monte Carlo simulations with identified uncertainty sources. (c) The core burning area was defined by a minimum dNBR threshold of 0.2.

core burn area, 0.08 within the entire fire scar, and 0.11 outside the fire scar. Unburned deciduous cover exhibited the greatest variability.

Spring albedo showed the expected response to burning (Figure S5). The mean increase was 0.23 within the core burn area, 0.16 within the fire perimeter, and −0.01 outside the fire scar. Changes in spring albedo and dNBR were highly correlated within the fire perimeter ($r = 0.87$). The total number of layers for spring albedo anomalies varied between 3 and 20 within the fire scar.

Our fractional deciduous layer compared favorably with a domain-wide map of vegetation type from LANDFIRE (Figure 7). It also performed well at our field sites: seven of the eight sites with the highest mapped deciduous fraction were white spruce-aspen stands.

3.3. Modeling Carbon Emissions

We fit a model of combustion at the field sites based on two terms: (1) transformed dNBR and (2) the product of dNBR and deciduous fraction derived from our spectral unmixing model (Figure 6). The resulting equation was

$$C = 0.935 \times f(\mathrm{dNBR}_N) + 13.7 \times \mathrm{dNBR}_A \times \mathrm{D} \quad (3)$$

where C = combustion (kg C m^{-2}), $\mathrm{dNBR_N}$ = dNBR normalized by the mean at control sites (0.098), dNBR_A = dNBR adjusted by applying a maximum threshold of 0.85, and D = deciduous fraction with a maximum of 0.25. Combustion in pixels with dNBR_N less than or equal to the maximum at control sites (0.036) was set to zero. Combustion was capped at a maximum of 1.2 times the maximum from burned sites (5.30 kg C m^{-2}). The function f represents the inverse logistic transformation of $\mathrm{dNBR_N}$:

$$f(\mathrm{dNBR}_N) = 0.718 \times \ln\left(\frac{\mathrm{dNBR}_N + 0.334}{0.982 - \mathrm{dNBR}_N}\right) + 0.805 \quad (4)$$

Although increases in dNBR tended to saturate with combustion levels greater than approximately 2.5 kg C m^{-2}, the regression performed relatively well at the field sites (Figure 6). The resulting model adequately adjusted for the different relationships between dNBR and combustion in black spruce versus white spruce-aspen sites, contained no observable bias, and produced an r^2 value of 0.84 for total combustion when all sites were considered. Fits for belowground were similar ($r^2 = 0.82$). Because the model did not perform as well for aboveground combustion, this was taken as the difference between total and belowground. The dNBR-based model was applied at every 30 m pixel within the fire scar to estimate landscape-scale carbon emissions (Figure 8). Total emissions were estimated to be 158 ± 27 Gg C, with 94% coming from the core burn area. Mean combustion inside the core burn area was slightly lower than the mean at field sites (2.67 ± 0.40 kg C m^{-2} versus 2.88 ± 0.23, Table 2) (Unless otherwise stated, uncertainties

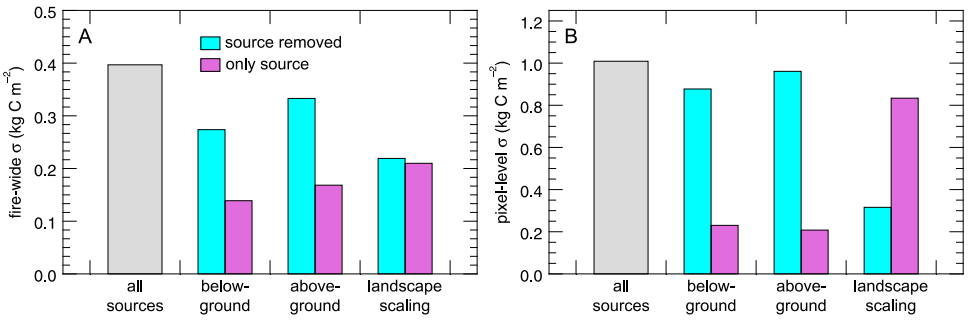

Figure 9. Attribution of uncertainty sources for (a) fire-wide and (b) pixel-level standard error of combustion in the core burn area. Sources were categorized by belowground combustion, aboveground combustion, and landscape scaling. For each source category we performed two additional sets of 1000 Monte Carlo simulations: one where the values and methods for the source category were held constant as in the main approach ("source removed") and one where the category was the only contributing factor ("only source"). Our modeling approach lead to comparatively high pixel-level errors that were largely averaged out across the fire perimeter.

for the fire scar represent one standard error for fire-wide estimates. Site-level uncertainties represent one standard error across all burned sites). Mean combustion across the entire fire scar, however, was notably lower due to lower severity areas and unburned islands (1.98 ± 0.34 kg C m^{-2}) (Table 2 and Figure S4).

Combustion levels in white spruce-aspen forests were slightly higher than black spruce (19% higher at field sites, 11% higher in the core burn area, and 3% higher across the perimeter) (Table 2). Because of spatial coverage, however, black spruce forests contributed the majority (67 ± 16%) of total emissions, followed by white spruce-aspen forests (19 ± 4%), shrubs (7%), and pure deciduous forests (5%). Deciduous cover appeared to stop the spread of fire in many locations and constituted a relatively large fraction of low-severity or unburned patches: 23% within the core burn area versus 48% outside of it based on our fractional deciduous layer (Figure 7a).

Increases in spring albedo also yielded significant relationships with site-level combustion, although with higher uncertainties (Figure S5). Using a similar approach as described above for dNBR, this albedo-driven model produced an r^2 value of 0.76 for all sites. Mean combustion was estimated to be 2.62 ± 0.41 kg C m^{-2} within the core burn area and 2.03 ± 0.35 kg C m^{-2} across the fire scar. Spatial patterns were similar but not identical to the dNBR-based model ($r = 0.80$).

For comparison with previous work we report that CBI and dNBR were strongly correlated: $r^2 = 0.78$ using all burned sites and 0.91 in burned black spruce. However, CBI saturated more quickly than dNBR and was not useful in discriminating between sites with combustion greater than approximately 2 kg C m^{-2} (Figure S6).

3.4. Uncertainties

Uncertainties were derived from Monte Carlo simulations with varied parameters and methodological choices for belowground combustion, aboveground combustion, and landscape scaling (section 2.8). All reported uncertainties are for fire-wide means. Systemic errors (i.e., modified many values in a given Monte Carlo run by a similar direction and magnitude) altered the nature of our regression model (Figure 6) and had the greatest impact on fire-wide uncertainty. Contributions from systemic errors were relatively similar for the three source categories (Figure 9a), totaling 0.40 kg C m^{-2} for the standard error in combustion within the core burn area. However, uncertainty ranges at any given pixel were substantially larger (1.01 kg C m^{-2} for the pooled pixel-level standard error) (Figures 8 and 9b). This inflation of pixel-level uncertainty was mainly due to the implementation of prediction error in our regression model, which varied randomly for every pixel but was largely averaged out for fire-wide means.

4. Discussion

Fuel consumption in boreal forest fires depends on a number of biotic and abiotic factors, including tree species, stand age and density, understory composition, drainage, slope and aspect, meteorology, and timing

Journal of Geophysical Research: Biogeosciences 10.1002/2014JG002657

Table 3. Previous Combustion Estimates in Alaska and Canada[a]

	Reference	Forest Type	Belowground Combustion (kg C m^{-2})	Total Combustion (kg C m^{-2})	Other Information[b]
Alaska field observations	*Kasischke et al.* [2000]	black spruce	3.4 (1.4–7.6)	4.3	range based on field sites, higher combustion from later-season burns
	Michalek et al. [2000]	black spruce (88%)		4.0 (1.6–10.8)	three severity and three tree density classes, scaled with Landsat to perimeter, range based on classes
	Boby et al. [2010]	black spruce	2.9 (0.1–6.8)	3.3 (1.5–4.6)	range based on field sites
	This study	**black spruce**	**1.85 (1.6–2.1)**	**2.6 (2.3–3.0)**	**range based on standard error of the mean in core burn area**
	Neff et al. [2005]; *Randerson et al.* [2006a]	black spruce	1.2 (1.1–1.4)	1.6 (1.4–1.7)	range based on methods
	Kasischke and Johnstone [2005]	black spruce	0.6–5.7		range based on field sites, higher combustion from later-season burns
	Dyrness and Norum [1983]	black spruce	0.8–4.7		experimental crown fires, range based on severity
	Kane et al. [2007]	black spruce	3.3–4.0		range based on topography
	Harden et al. [2006]	black spruce	1.7		
	Harden et al. [2004]	black spruce	0.5–0.9		experimental fire, range based on soil profiles
	Kasischke et al. [2000]	willow-black spruce	1.2	1.4	
	Kasischke et al. [2000]	white spruce	2.0	2.6	
	This study	**white spruce-aspen**	**2.1 (1.8–2.3)**	**2.9 (2.5–3.4)**	
	Kasischke et al. [2000]	aspen	0.9	1.4	
Alaska modeling	*Kasischke et al.* [2000]	black spruce		1.2–4.2	range based on severity scenarios
	French et al. [2000]	mixed	3.2	3.8	field data + ecozones
	French et al. [1996]	mixed		3.3	conceptual model based on field measurements, timing and site conditions
	Kasischke et al. [1995]	mixed		2.5–3.0	field data + model of age-based biomass, range based on years and burn area estimates
	Kasischke and Hoy [2012]	mixed	1.3–2.6	1.7–3.0	range based on small and large fire years, model based on fuel types, topography, fire weather
	French et al. [2002]	mixed		0.9–3.0	field data + severity scenarios, range based on scenarios
Canada field observations	*Stocks and Kauffman* [1997]	spruce		1.0[c]	experimental crown fires
	Alexander et al. [1991]	black spruce	0.5[c]	0.7[c]	experimental fires
	Stocks et al. [2004]	jack pine, black spruce	0.7 (0.5–1.1)[c]	1.9 (1.7–2.4)[c]	experimental crown fires
	Stocks [1987]	immature jack pine	0.6 (0.3–01.0)[c]	1.0 (0.4–1.4)[c]	experimental, mostly crown fires

Table 3. (continued)

	Reference	Forest Type	Belowground Combustion (kg C m^{-2})	Total Combustion (kg C m^{-2})	Other Information[b]
	Quintilio et al. [1977]	jack pine	0.5 (0.3–0.6)[c]	0.9 (0.6–1.4)[c]	experimental fires
	Stocks [1989]	mature jack pine	0.4 (0.2–0.6)[c]	0.5 (0.2–1.1)[c]	experimental, mix of surface and crown fires
	de Groot et al. [2009]	mixed		1.4 (0.3–2.4)	range based on field sites
	Stocks and Kauffman [1997]	mixed		0.8–2.0[c]	
Canada modeling	*de Groot et al.* [2007]	spruce		1.6–2.2	BORFIRE + Canadian FBP System, range based on models
	de Groot et al. [2007]	immature pine		1.5–1.6	
	de Groot et al. [2007]	mature pine		1.1–1.6	
	Kasischke and Bruhwiler [2002]	mixed		0.9–3.7[d]	Eastern, Central, and Western boreal North America, severity scenarios
	French et al. [2000]	mixed	0.3–2.3	0.5–2.7	field data + ecozones, range based on ecozones
	Kasischke et al. [2005]	mixed		0.7–2.6[d]	range based on years and severity scenarios
	Amiro et al. [2001]	mixed	1.1	1.3 (0.5–2.0)	range based on ecozones, model based on fire weather
	de Groot et al. [2007]	mixed		0.6–1.7	
	de Groot et al. [2007]	deciduous trees		0.5–1.7	

[a]Bold is used to highlight values from this study.
[b]Unless otherwise stated, assumed to be wildfire.
[c]When reported separately, belowground fuel was assumed to have a carbon concentration of 0.4 and aboveground was assumed to have a carbon concentration of 0.45. Otherwise, all fuel was assumed to have a carbon concentration of 0.4.
[d]Includes both Canada and Alaska.

of a burn within a season. As a result, combustion levels cover a wide range within and across fire complexes (Table 3). Experimental fires tend to be less severe than wildfires, primarily because of the less severe fire weather in which experimental fires are typically conducted. Generally, deeper duff layers in the forests of interior Alaska lead to greater combustion than those in Canada. Large fire years and later season burns also tend to be more severe due to deeper burning of the forest floor [*Kasischke et al.*, 2000; *Kasischke and Johnstone*, 2005; *Turetsky et al.*, 2011].

Our reported combustion for the 2010 Gilles Creek fire lies in the middle of the range when compared to previous estimates for interior Alaska (Table 3). We also report somewhat higher fractional emissions from aboveground pools ($29 \pm 5\%$ at field sites and $31 \pm 6\%$ across the fire scar) compared to previous work [*Kasischke et al.*, 2000; *Amiro et al.*, 2001; *Boby et al.*, 2010; *Kasischke and Hoy*, 2012]. Soil combustion in Gilles Creek may have been comparatively moderate because it was an early season burn (late May/early June) on primarily south facing terrain, which typically contains lower soil carbon stocks compared to other topographic positions [*Kane et al.*, 2007]. We note that mean combustion in Gilles Creek closely matched the early season black spruce burn estimates from *Kasischke and Hoy* [2012].

The majority of emissions from boreal fires in North America, especially those in Alaska, come from the forest floor. It has been argued that spectral indices are not particularly useful in predicting these emissions because the dominant signal in visible, near-infrared, and shortwave infrared wavelengths comes from the canopy [*Roy et al.*, 2006; *French et al.*, 2008; *Hoy et al.*, 2008; *Murphy et al.*, 2008]. However, more intense crown fires are expected to combust more of the tree canopy and induce greater radiative heating and therefore drying of the surface layers. They are also generally associated with more intense surface

fires, thus burning deeper into the forest floor [*Ryan*, 2002; *Alexander and Cruz*, 2012]. Greater belowground combustion therefore likely correlates with properties that influence spectral wavelengths, including surface char, tree consumption, tree fall, surface water content, and stand density. As an example, belowground and aboveground combustion were positively correlated at our field sites (Figure S3).

We show that after accounting for forest type, heterogeneity in duff consumption, and atmospheric and terrain influences on surface reflectance, spectral indices from fine-scale imagery (30 m) may be useful in estimating total combustion in interior Alaska. This agrees with *Barrett et al*. [2011], who found that dNBR and the ratio of Landsat bands 7 to 5 were among the top nine of 35 predictors of burn depth across fire complexes in Alaska. The remaining top predictors, including metrics of topography and meteorology, are not expected to have varied substantially between our field sites. Our work also agrees with *Hudak et al*. [2007], who found that NBR and dNBR exhibited relatively high explanatory power for total and surface organic char in interior Alaska.

Because of dNBR saturation with combustion greater than approximately 2.5 kg C m^{-2}, we note that our approach may not be as useful in fires that consistently consume more of the forest floor and emit significantly higher levels of carbon. However, combustion levels in many fires in Alaska and Canada are within the range where spectral indices would be valuable for modeling (Table 3). We also found that depth of burn from 87 previously reported black spruce field sites [*Turetsky et al*., 2011] displayed a similar logistic relationship with dNBR as those in Gilles Creek, although with much higher variance: $r^2 = 0.78$ for burned black spruce sites in our study versus 0.31 for the Turetsky data (Figure S7). While site and meteorological conditions at the time of burn were relatively similar across our field sites, these are generally not across fire complexes and introduce considerable scatter to the relationship between dNBR and combustion.

The dNBR-combustion relationship was also considerably different for black spruce and white spruce-aspen stands. This is predominantly related to differences in canopy versus ground-layer combustion. All black spruce trees were killed in medium- and high-severity sites, and their canopies were nearly completely consumed. White spruce-aspen forests, on the other hand, contained greater aboveground biomass but experienced significantly less fractional consumption (Figure 3). Because dNBR is strongly influenced by canopy dynamics, black spruce forests exhibited a larger dNBR for a given combustion level (Figure 6).

We provide for the first time estimates of uncertainty in emissions stemming from a wide array of methodological sources. Results indicated an approximate 15% error in fire-wide estimates and 38% error for any given pixel. Site-level combustion and our modeling approach contributed relatively equally to errors in fire-wide means. In contrast, most of the uncertainty for any given pixel came from model errors. Despite contributing to approximately 70% of emissions, uncertainty in belowground combustion was similar to aboveground. We attribute this to our (1) careful focus on the quantification of soil combustion and (2) assignment of systemic errors for aboveground methodology due to fewer direct measurements (Table S3).

In contrast to other methods, our approach makes direct quantitative use of fire severity observations. We build on previous work that utilized remote imagery to upscale carbon emissions to a fire perimeter [*Michalek et al*., 2000]. While this study demonstrated utility for the general approach, it was based on relatively little data from burned sites, made considerable assumptions about consumption efficiency, did not report metrics of model performance, and is difficult to directly apply to other fires because of site-specific image classification techniques. We also found that increases in spring albedo may be a viable alternative for modeling carbon emissions in these forests. This may be helpful when cloud contamination prevents the use of summer imagery. We note, however, that this metric may need to be optimized for individual regions because of variations in snow depth and species-specific differences in stand density and height. The inclusion of nonspectral data streams, including topographic effects, seasonal fire weather, and meteorology at the time of burn, may better constrain emissions across multiple fire complexes, given appropriate validation data.

Our study highlights the importance of low-severity areas and unburned islands within a fire perimeter. Despite having deliberately sought out lower severity field sites, mean combustion across the fire perimeter was 31% lower than the site-level average. This likely applies to other fires in the region. The MTBS database includes dNBR-based fire severity categories for every perimeter in Alaska beginning in 1984. These categories differ substantially by combustion for the Gilles Creek fire: mean combustion was 3.0 kg C m^{-2} in high-severity areas, 2.8 kg C m^{-2} in moderate severity, 2.0 kg C m^{-2} in low severity, 0.6 kg C m^{-2} in unburned–low severity, and 0.0 kg C m^{-2} in areas of increased greenness. The latter two categories covered

36.2% and 0.3% of the Gilles Creek fire perimeter. Including all fires in Alaska between 1984 and 2011 from the MTBS database, 16.6% of burn perimeters were classified as unburned–low severity and 0.8% as increased greenness. This agrees with *Sedano and Randerson* [2014], who estimated that 15% of the area inside large fire perimeters (those contributing to 95% of the burn area) during 2000–2010 were unburned islands. It also agrees with *Kolden et al.* [2012], who showed that unburned islands comprised 14–37% of fire perimeters in three western U.S. national parks during 1984–2009. We note that many of the low-severity areas in the Gilles Creek burn were dominated by deciduous vegetation (Figures 7 and 8). This implies that deciduous trees and shrubs suppressed the spread of fire and confirms previous work on the flammability of boreal conifers versus deciduous broadleaf trees [*Dyrness et al.*, 1986; *Hely et al.*, 2000; *Krawchuk et al.*, 2006; *Beck et al.*, 2011].

Models of biomass burning are generally applied to fire perimeters after being trained on field observations of combustion. However, this approach neglects the influence of unburned islands and particularly low-severity patches, which are likely underrepresented in field estimates, including our own. Our analysis suggests that these low-severity or unburned areas can be influential for estimates of fire-wide emissions, especially for models using these or similar fire perimeters. Burn area estimates based directly on reflectance changes are frequently lower and may compensate for this effect. For example, the Global Fire Emissions Database (GFED) version 3 including small fires [*Randerson et al.*, 2012] estimates a mean combustion of 3.05 kg C m^{-2} for the Gilles Creek burn. This is relatively close to our field estimates and mean within the core burn but is substantially higher than the mean across the fire perimeter (1.98 ± 0.34 kg C m^{-2}). However, GFED also underestimates burn area at Gilles Creek by 50% compared to the MTBS fire scar, so the model's total carbon emissions are 22% lower than our estimates.

One limitation of our study involves our sampling approach, which focused only on black spruce and white spruce-aspen forests. Site accessibility is a major challenge in obtaining field measurements from remote locations. As a consequence, we were not able to sample any pure deciduous stands. White spruce-aspen sites that we sampled generally contained shallower but more compact soils (Figure 2) with greater fractional consumption than black spruce. Although many of the aspen trees did not show signs of crown fires, white spruce did, and mean site-level aboveground combustion was similar because of the larger trees. Taken together, our data suggested that white spruce-aspen forests could emit a similar amount of carbon with lower dNBR signals (Figure 6). Because we used a continuous layer of deciduous fraction to account for these mixed forests when scaling, some of the areas with greatest modeled combustion (particularly in the northwest) exhibited combined dNBR and deciduous fractions greater than levels seen at our field sites (Figures 5, 7, and 8). Deciduous stands, however, generally contain shallower organic soil horizons than mixed stands [*Kasischke et al.*, 2000; *Turetsky et al.*, 2005; *de Groot et al.*, 2007], and thus, our estimates may be biased high in these regions. We also sampled a relatively low number of low-severity and white spruce-aspen stands, which adds to uncertainty across the perimeter.

We were unable to sample sites dominated by shrubs, which occupied 13% of the fire scar based on LANDFIRE, or any burned black spruce stands underlain by deep organic soils with permafrost. The latter may have occupied southern stretches of the fire scar based on maps of slope and vegetation type. However, although they contain much larger soil carbon stocks, these lowland forests have been shown to experience less fractional consumption and generally emit similar amounts of carbon compared to upland black spruce [*Kane et al.*, 2007; *Shetler et al.*, 2008]. We did not quantify combustion of coarse woody debris and roots. Although combustion from coarse woody debris may be substantial in southern boreal forests [*de Groot et al.*, 2007], our control sites contained very few, if any, of this material. Our sampled stands also showed no signs of understory shrubs. Some amount of error is always associated with image processing, including atmospheric and terrain corrections. Additionally, our choice of metric (dNBR) and year undoubtedly influenced the results. For example, using 1 year postfire (2011) instead of the year-of-fire (2010) for the calculation of dNBR, i.e., extended versus initial analysis, resulted in a 6% decrease in emissions within the core burn area and 9% within the fire scar. We made a number of additional assumptions in modeling fire-wide emissions, including how to treat deciduous vegetation and maximum allowable combustion.

Finally, we note that the Gilles Creek fire occurred earlier in the year than most others in Alaska and Canada [*Kasischke et al.*, 2002; *Stocks et al.*, 2003]. This may limit the applicability of our results to other fires because the forest floor was likely comparatively colder, wetter, and potentially more frozen. This may have suppressed the burning of deep organic layers, especially in black spruce stands, resulting in a higher

variability and lower mean combustion. Regression parameters are likely different for later-season burns, and the saturation of dNBR and similar indices may be worse in higher-severity fires that consistently burn deeper into the forest floor. However, the surface water and ice content of the soil organic matter in late spring/early summer varies interannually as a function of snowpack, timing of thaw, and climate [*Granberg et al*., 1999; *Welp et al*., 2007]. Given the frequency of deep burning observed in Gilles Creek sites, it is likely that much of the ground was unfrozen or easily thawed at the time of burn.

5. Conclusions

Accurate estimates of carbon emissions from increasingly frequent boreal forest fires are crucial for understanding and projecting high-latitude climate feedbacks. Our dNBR-based emission estimates and uncertainties across the Gilles Creek fire can be used to constrain larger-scale models, and our integration of remote sensing and field measurements offers a complimentary approach to existing methods. A number of factors are crucial to the method's implementation: (1) careful quantification of both soil and canopy combustion, (2) sampling at lower severity field sites, (3) accounting for distinct forest types, and (4) appropriate corrections for atmospheric contamination and terrain effects. This approach may prove useful in other biomes and vegetation types, particularly those with mixed fire regimes (i.e., surface versus crown).

Important next steps are to validate our approach for other fires and regions and to incorporate additional nonspectral data sources. Our work suggests that relationships between fire severity and spectral indices may help constrain burning conditions in emissions models. If properly implemented, future developments have the potential to greatly reduce uncertainty in large-scale fire emissions.

Acknowledgments

This work was funded by a U.S. National Science Foundation Graduate Research Fellowship (ID 2009067341) to B.M.R. and the NASA Carbon in Arctic Reservoirs Vulnerability Experiment (CARVE) to J.T.R. We thank M. Waldrop (USGS, Menlo Park) and M. Goulden (UC Irvine) for assisting with field equipment, J. Miu and D. Sandusky (UC Irvine) for homogenizing and preparing soil samples, and D. Zhang (UC Irvine) for analyzing carbon concentrations. We are grateful to the Alaska Department of Natural Resources and the Pogo Gold Mine, operated by Sumitomo Metal Mining Co., for road access to the field sites. Readers may access additional data used in the publication by contacting the authors.

References

Alexander, M. E., and M. G. Cruz (2012), Interdependencies between flame length and fireline intensity in predicting crown fire initiation and crown scorch height, *Int. J. Wildland Fire*, *21*(2), 95–113, doi:10.1071/WF11001.

Alexander, M. E., B. J. Stocks, and B. D. Lawson (1991), *Fire Behavior in Black Spruce-Lichen Woodland: The Porter Lake Project*, Forestry Canada, Northwest Region, Northern Forestry Centre, Edmonton, Alberta, Canada.

Allen, J. L., and B. Sorbel (2008), Assessing the differenced Normalized Burn Ratio's ability to map burn severity in the boreal forest and tundra ecosystems of Alaska's national parks, *Int. J. Wildland Fire*, *17*(4), 463–475, doi:10.1071/WF08034.

Amiro, B. D., J. B. Todd, B. M. Wotton, K. A. Logan, M. D. Flannigan, B. J. Stocks, J. A. Mason, D. L. Martell, and K. G. Hirsch (2001), Direct carbon emissions from Canadian forest fires, 1959–1999, *Can. J. For. Res.*, *31*(3), 512–525, doi:10.1139/cjfr-31-3-512.

Bachelet, D., J. Lenihan, R. Neilson, R. Drapek, and T. Kittel (2005), Simulating the response of natural ecosystems and their fire regimes to climatic variability in Alaska, *Can. J. For. Res.*, *35*(9), 2244–2257, doi:10.1139/X05-086.

Balshi, M. S., A. D. McGuire, P. Duffy, M. Flannigan, J. Walsh, and J. Melillo (2009), Assessing the response of area burned to changing climate in western boreal North America using a Multivariate Adaptive Regression Splines (MARS) approach, *Global Change Biology*, *15*(3), 578–600, doi:10.1111/j.1365-2486.2008.01679.x.

Barney, R., K. Vancleve, and R. Schlentner (1978), Biomass distribution and crown characteristics in 2 Alaskan Picea-Mariana ecosystems, *Can. J. For. Res.*, *8*(1), 36–41, doi:10.1139/x78-007.

Barrett, K., E. S. Kasischke, A. D. McGuire, M. R. Turetsky, and E. S. Kane (2010), Modeling fire severity in black spruce stands in the Alaskan boreal forest using spectral and non-spectral geospatial data, *Remote Sens. Environ.*, *114*(7), 1494–1503, doi:10.1016/j.rse.2010.02.001.

Barrett, K., A. D. McGuire, E. E. Hoy, and E. S. Kasischke (2011), Potential shifts in dominant forest cover in interior Alaska driven by variations in fire severity, *Ecol. Appl.*, *21*(7), 2380–2396, doi:10.1890/10-0896.1.

Beck, P. S. A., S. J. Goetz, M. C. Mack, H. D. Alexander, Y. Jin, J. T. Randerson, and M. M. Loranty (2011), The impacts and implications of an intensifying fire regime on Alaskan boreal forest composition and albedo, *Global Change Biology*, *17*, 2853–2866, doi:10.1111/j.1365-2486.2011.02412.x.

Boby, L. A., E. A. G. Schuur, M. C. Mack, D. Verbyla, and J. F. Johnstone (2010), Quantifying fire severity, carbon, and nitrogen emissions in Alaska's boreal forest, *Ecol. Appl.*, *20*(6), 1633–1647, doi:10.1890/08-2295.1.

Brewer, C. K., J. C. Winne, R. L. Redmond, D. W. Opitz, and M. V. Mangrich (2005), Classifying and mapping wildfire severity: A comparison of methods, *Photogramm. Eng. Remote Sens.*, *71*(11), 1311–1320.

Campbell, J., D. C. Donato, D. Azuma, and B. Law (2007), Pyrogenic carbon emission from a large wildfire in Oregon, United States, *J. Geophys. Res.*, *112*, G04014, doi:10.1029/2007JG000451.

Chapin, F. S., III, T. Hollingsworth, D. F. Murray, L. A. Viereck, and M. D. Walker (2006), Successional processes in the Alaskan boreal forest, in *Alaska's Changing Boreal Forest*, edited by F. S. Chapin III et al., pp. 100–120, Oxford Univ. Press, New York.

Chuvieco, E., and R. G. Congalton (1988), Mapping and inventory of forest fires from digital processing of TM data, *Geocarto Int.*, *3*(4), 41–53.

De Groot, W. J., et al. (2007), Estimating direct carbon emissions from Canadian wildland fires, *Int. J. Wildland Fire*, *16*(5), 593–606, doi:10.1071/WF06150.

De Groot, W. J., J. M. Pritchard, and T. J. Lynham (2009), Forest floor fuel consumption and carbon emissions in Canadian boreal forest fires, *Can. J. For. Res.*, *39*(2), 367–382, doi:10.1139/X08-192.

DeFries, R., M. Hansen, and J. Townshend (1995), Global discrimination of land cover types from metrics derived from AVHRR pathfinder data, *Remote Sens. Environ.*, *54*(3), 209–222, doi:10.1016/0034-4257(95)00142-5.

Dyrness, C., and R. Norum (1983), The effects of experimental fires on black spruce forest floors in interior Alaska, *Can. J. For. Res.*, *13*(5), 879–893, doi:10.1139/x83-118.

Dyrness, C. T., L. A. Viereck, and K. Van Cleve (1986), Fire in Taiga Communities of Interior Alaska, in *Forest Ecosystems in the Alaskan Taiga*, edited by K. Van Cleve et al., pp. 74–86, Springer, New York.

Eidenshink, J., B. Schwind, K. Brewer, Z.-L. Zhu, B. Quayle, and S. Howard (2007), A project for monitoring trends in burn severity, *Fire Ecol.*, *3*(1), 3–20.

Epting, J., D. Verbyla, and B. Sorbel (2005), Evaluation of remotely sensed indices for assessing burn severity in interior Alaska using Landsat TM and ETM+, *Remote Sens. Environ.*, *96*(3–4), 328–339, doi:10.1016/j.rse.2005.03.002.

Euskirchen, E. S., A. D. McGuire, T. S. Rupp, F. S. Chapin III, and J. E. Walsh (2009), Projected changes in atmospheric heating due to changes in fire disturbance and the snow season in the western Arctic, 2003–2100, *J. Geophys. Res.*, *114*, G04022, doi:10.1029/2009JG001095.

Eva, H., and E. F. Lambin (1998), Burnt area mapping in Central Africa using ATSR data, *Int. J. Remote Sens.*, *19*(18), 3473–3497, doi:10.1080/014311698213768.

Fauria, M. M., and E. A. Johnson (2008), Climate and wildfires in the North American boreal forest, *Philos. Trans. R. Soc. B. Biol. Sci.*, *363*(1501), 2317–2329, doi:10.1098/rstb.2007.2202.

Flannigan, M., B. Stocks, M. Turetsky, and M. Wotton (2009), Impacts of climate change on fire activity and fire management in the circumboreal forest, *Global Change Biology*, *15*(3), 549–560, doi:10.1111/j.1365-2486.2008.01660.x.

French, N., E. Kasischke, R. Johnson, L. Bourgeau-Chavez, A. Frick, and S. Ustin (1996), Estimating fire-related carbon flux in Alaska boreal forests using multi-sensor remote sensing data, in *Biomass Burning and Climatic Change*, vol. 2, edited by J. Levine, pp. 808–826, MIT Press, Cambridge, Mass.

French, N. H. F., E. S. Kasischke, B. J. Stocks, J. P. Mudd, D. L. Martell, and B. S. Lee (2000), Carbon release from fires in the North American boreal forest, in *Fire, Climate Change, and Carbon Cycling in the Boreal Forest*, edited by E. S. Kasischke and B. J. Stocks, pp. 377–388, Springer, New York.

French, N. H. F., E. S. Kasischke, and D. G. Williams (2002), Variability in the emission of carbon-based trace gases from wildfire in the Alaskan boreal forest, *J. Geophys. Res.*, *108*(D1), 8151, doi:10.1029/2001JD000480.

French, N. H. F., E. S. Kasischke, R. J. Hall, K. A. Murphy, D. L. Verbyla, E. E. Hoy, and J. L. Allen (2008), Using Landsat data to assess fire and burn severity in the North American boreal forest region: An overview and summary of results, *Int. J. Wildland Fire*, *17*(4), 443–462, doi:10.1071/WF08007.

French, N. H. F., et al. (2011), Model comparisons for estimating carbon emissions from North American wildland fire, *J. Geophys. Res.*, *116*, G00K05, doi:10.1029/2010JG001469.

Granberg, G., H. Grip, M. O. Lofvenius, I. Sundh, B. H. Svensson, and M. Nilsson (1999), A simple model for simulation of water content, soil frost, and soil temperatures in boreal mixed mires, *Water Resour. Res.*, *35*(12), 3771–3782, doi:10.1029/1999WR900216.

Hall, R. J., J. T. Freeburn, W. J. de Groot, J. M. Pritchard, T. J. Lynham, and R. Landry (2008), Remote sensing of burn severity: Experience from western Canada boreal fires, *Int. J. Wildland Fire*, *17*(4), 476–489, doi:10.1071/WF08013.

Harden, J. W., J. C. Neff, D. V. Sandberg, M. R. Turetsky, R. Ottmar, G. Gleixner, T. L. Fries, and K. L. Manies (2004), Chemistry of burning the forest floor during the FROSTFIRE experimental burn, interior Alaska, 1999, *Glob. Biogeochem. Cycles*, *18*, GB3014, doi:10.1029/2003GB002194.

Harden, J. W., K. L. Manies, M. R. Turetsky, and J. C. Neff (2006), Effects of wildfire and permafrost on soil organic matter and soil climate in interior Alaska, *Global Change Biology*, *12*(12), 2391–2403, doi:10.1111/j.1365-2486.2006.01255.x.

Hely, C., Y. Bergeron, and M. D. Flannigan (2000), Effects of stand composition on fire hazard in mixed-wood Canadian boreal forest, *J. Veg. Sci.*, *11*(6), 813–824, doi:10.2307/3236551.

Hess, J. C., C. A. Scott, G. L. Hufford, and M. D. Fleming (2001), El Niño and its impact on fire weather conditions in Alaska, *Int. J. Wildland Fire*, *10*(1), 1–13, doi:10.1071/WF01007.

Hijmans, R. J., S. E. Cameron, J. L. Parra, P. G. Jones, and A. Jarvis (2005), Very high resolution interpolated climate surfaces for global land areas, *Int. J. Climatol.*, *25*(15), 1965–1978, doi:10.1002/joc.1276.

Hoy, E. E., N. H. F. French, M. R. Turetsky, S. N. Trigg, and E. S. Kasischke (2008), Evaluating the potential of Landsat TM/ETM + imagery for assessing fire severity in Alaskan black spruce forests, *Int. J. Wildland Fire*, *17*(4), 500–514, doi:10.1071/WF08107.

Hudak, A. T., P. Morgan, M. J. Bobbitt, A. M. S. Smith, S. A. Lewis, L. B. Leintile, P. R. Robichaud, J. T. Clark, and R. A. McKinley (2007), The relationship of multispectral satellite imagery to immediate fire effects, *J. Fire Ecol.*, *3*, 64–90.

Irish, R. R., J. L. Barker, S. N. Goward, and T. Arvidson (2006), Characterization of the Landsat-7 ETM+ Automated Cloud-Cover Assessment (ACCA) algorithm, *Photogramm. Eng. Remote Sens.*, *72*(10), 1179–1188.

Jin, Y., J. T. Randerson, S. J. Goetz, P. S. A. Beck, M. M. Loranty, and M. L. Goulden (2012), The influence of burn severity on postfire vegetation recovery and albedo change during early succession in North American boreal forests, *J. Geophys. Res.*, *117*, G01036, doi:10.1029/2011JG001886.

Kane, E. S., E. S. Kasischke, D. W. Valentine, M. R. Turetsky, and A. D. McGuire (2007), Topographic influences on wildfire consumption of soil organic carbon in interior Alaska: Implications for black carbon accumulation, *J. Geophys. Res.*, *112*, G03017, doi:10.1029/2007JG000458.

Kasischke, E. S., and L. P. Bruhwiler (2002), Emissions of carbon dioxide, carbon monoxide, and methane from boreal forest fires in 1998, *J. Geophys. Res.*, *108*(D1), 8146, doi:10.1029/2001JD000461.

Kasischke, E. S., and E. E. Hoy (2012), Controls on carbon consumption during Alaskan wildland fires, *Global Change Biology*, *18*(2), 685–699, doi:10.1111/j.1365-2486.2011.02573.x.

Kasischke, E. S., and J. F. Johnstone (2005), Variation in postfire organic layer thickness in a black spruce forest complex in interior Alaska and its effects on soil temperature and moisture, *Can. J. For. Res.*, *35*(9), 2164–2177, doi:10.1139/X05-159.

Kasischke, E. S., K. P. O'Neill, N. H. F. French, and L. L. Bourgeau-Chavez (2000), Controls on patterns of biomass burning in Alaskan boreal forests, in *Fire, Climate Change, and Carbon Cycling in the Boreal Forest*, edited by E. S. Kasischke and B. J. Stocks, pp. 173–196, Springer, New York.

Kasischke, E. S., D. Barry, and D. Williams (2002), Analysis of the patterns of large fires in the boreal forest region of Alaska, *Int. J. Wildland Fire*, *11*(2), 131–144, doi:10.1071/WF02023.

Kasischke, E. S., E. J. Hyer, P. C. Novelli, L. P. Bruhwiler, N. H. F. French, A. I. Sukhinin, J. H. Hewson, and B. J. Stocks (2005), Influences of boreal fire emissions on Northern Hemisphere atmospheric carbon and carbon monoxide, *Glob. Biogeochem. Cycles*, *19*, GB1012, doi:10.1029/2004GB002300.

Kasischke, E. S., M. R. Turetsky, R. D. Ottmar, N. H. F. French, E. E. Hoy, and E. S. Kane (2008), Evaluation of the composite burn index for assessing fire severity in Alaskan black spruce forests, *Int. J. Wildland Fire*, *17*(4), 515–526, doi:10.1071/WF08002.

Kasischke, E. S., et al. (2010), Alaska's changing fire regime implications for the vulnerability of its boreal forests, *Can. J. For. Res.*, *40*(7), 1313–1324, doi:10.1139/X10-098.

Kasischke, E., N. French, L. Bourgeauchavez, and N. Christensen (1995), Estimating release of carbon from 1990 and 1991 forest-fires in Alaska, *J. Geophys. Res.*, *100*(D2), 2941–2951, doi:10.1029/94JD02957.

Keeley, J. E. (2009), Fire intensity, fire severity and burn severity: A brief review and suggested usage, *Int. J. Wildland Fire*, *18*(1), 116–126, doi:10.1071/WF07049.

Key, C. H., and N. C. Benson (2005), Landscape assessment: Ground measure of severity, the Composite Burn Index, and remote sensing of severity, the Normalized Burn Index, in *FIREMON: Fire Effects Monitoring and Inventory System*, edited by D. C. Lutes et al., pp. 1–55, U.S.D.A. Forest Service, Rocky Mountain Research Station, Ogden, UT.

Kolden, C. A., J. A. Lutz, C. H. Key, J. T. Kane, and J. W. van Wagtendonk (2012), Mapped versus actual burned area within wildfire perimeters: Characterizing the unburned, *For. Ecol. Manag.*, *286*, 38–47, doi:10.1016/j.foreco.2012.08.020.

Krawchuk, M. A., S. G. Cumming, M. D. Flannigan, and R. W. Wein (2006), Biotic and abiotic regulation of lightning fire initiation in the mixedwood boreal forest, *Ecology*, *87*(2), 458–468, doi:10.1890/05-1021.

Lebarron, R. (1945), Adjustment of black spruce root systems to increasing depth of peat, *Ecology*, *26*(3), 309–311, doi:10.2307/1932413.

Lentile, L. B., Z. A. Holden, A. M. S. Smith, M. J. Falkowski, A. T. Hudak, P. Morgan, S. A. Lewis, P. E. Gessler, and N. C. Benson (2006), Remote sensing techniques to assess active fire characteristics and post-fire effects, *Int. J. Wildland Fire*, *15*(3), 319–345, doi:10.1071/WF05097.

Liang, S. L. (2001), Narrowband to broadband conversions of land surface albedo I Algorithms, *Remote Sens. Environ.*, *76*(2), 213–238, doi:10.1016/S0034-4257(00)00205-4.

Mack, M. C., K. K. Treseder, K. L. Manies, J. W. Harden, E. A. G. Schuur, J. G. Vogel, J. T. Randerson, and F. S. Chapin (2008), Recovery of aboveground plant biomass and productivity after fire in mesic and dry black spruce forests of interior Alaska, *Ecosystems*, *11*(2), 209–225, doi:10.1007/s10021-007-9117-9.

Mamini, J., S. Siddiqui, and C. Barnwell (2008), *Alaska Statewide Digital Mapping Initiative*, Alaska Department of Natural Resources, HDR Alaska, Inc., Anchorage, Alaska. [Available at www.alaskamapped.org.] (Accessed 16 October 2013).

Manies, K. L., J. W. Harden, S. R. Silva, P. H. Briggs, and B. M. Schmid (2004), Soil data from *Picea mariana* stands near delta junction, Alaska of different ages and soil drainage type *U.S. Open File Rep., 2004–1271*, U.S. Geol. Surv., Department of the Interior, Anchorage, Alaska.

Masek, J. G., E. F. Vermote, N. E. Saleous, R. Wolfe, F. G. Hall, K. F. Huemmrich, F. Gao, J. Kutler, and T. K. Lim (2006), A Landsat surface reflectance dataset for North America, 1990–2000, *IEEE Geosci. Remote Sens. Lett.*, *3*(1), 68–72, doi:10.1109/LGRS.2005.857030.

McGuire, A. D., L. G. Anderson, T. R. Christensen, S. Dallimore, L. Guo, D. J. Hayes, M. Heimann, T. D. Lorenson, R. W. Macdonald, and N. Roulet (2009), Sensitivity of the carbon cycle in the Arctic to climate change, *Ecol. Monogr.*, *79*(4), 523–555, doi:10.1890/08-2025.1.

Michalek, J. L., N. H. F. French, E. S. Kasischke, R. D. Johnson, and J. E. Colwell (2000), Using Landsat TM data to estimate carbon release from burned biomass in an Alaskan spruce forest complex, *Int. J. Remote Sens.*, *21*(2), 323–338, doi:10.1080/014311600210858.

Miller, J. D., and A. E. Thode (2007), Quantifying burn severity in a heterogeneous landscape with a relative version of the delta Normalized Burn Ratio (dNBR), *Remote Sens. Environ.*, *109*(1), 66–80, doi:10.1016/j.rse.2006.12.006.

Miller, J. D., E. E. Knapp, C. H. Key, C. N. Skinner, C. J. Isbell, R. M. Creasy, and J. W. Sherlock (2009), Calibration and validation of the relative differenced Normalized Burn Ratio (RdNBR) to three measures of fire severity in the Sierra Nevada and Klamath Mountains, California, USA, *Remote Sens. Environ.*, *113*(3), 645–656, doi:10.1016/j.rse.2008.11.009.

Murphy, K. A., J. H. Reynolds, and J. M. Koltun (2008), Evaluating the ability of the differenced Normalized Burn Ratio (dNBR) to predict ecologically significant burn severity in Alaskan boreal forests, *Int. J. Wildland Fire*, *17*(4), 490–499, doi:10.1071/WF08050.

National Research Council (NRC) (2013), *Abrupt Impacts of Climate Change: Anticipating Surprises*, National Academies Press, Washington, D. C. [Available at http://www.nap.edu/openbook.php?record_id=18373&page=R1.]

Neff, J. C., J. W. Harden, and G. Gleixner (2005), Fire effects on soil organic matter content, composition, and nutrients in boreal interior Alaska, *Can. J. For. Res.*, *35*(9), 2178–2187, doi:10.1139/X05-154.

Nelson, R., R. Latty, and G. Mott (1984), Classifying northern forests using thematic mapper simulator data, *Photogramm. Eng. Remote Sens.*, *50*(5), 607–617.

Ottmar, R. D., S. J. Prichard, R. E. Vihnanek, D. V. Sandberg, and A. Bluhn (2006), *Modification and Validation of Fuel Consumption Models for Shrub and Forested Lands in the Southwest*, Pacific Northwest Research Station, Seattle, WA.

Quintilio, D., G. R. Fahnestock, and D. E. Dubé (1977), *Fire Behavior in Upland Jack Pine: The Darwin Lake Project*, Northern Forest Research Centre, Canadian Forestry Service, Environment Canada, Edmonton, Alberta.

Randerson, J. T., et al. (2006a), The impact of boreal forest fire on climate warming, *Science*, *314*(5802), 1130–1132, doi:10.1126/science.1132075.

Randerson, J. T., C. A. Masiello, C. J. Still, T. Rahn, H. Poorter, and C. B. Field (2006b), Is carbon within the global terrestrial biosphere becoming more oxidized? Implications for trends in atmospheric O-2, *Global Change Biology*, *12*(2), 260–271, doi:10.1111/j.1365-2486.2006.01099.x.

Randerson, J. T., Y. Chen, G. R. van der Werf, B. M. Rogers, and D. C. Morton (2012), Global burned area and biomass burning emissions from small fires, *J. Geophys. Res.*, *117*, G04012, doi:10.1029/2012JG002128. [Available at http://www.agu.org/pubs/crossref/2012/2012JG002128.shtml.] (Accessed 16 December 2012).

Reinhardt, E. D., R. E. Keane, and J. K. Brown (1997), *First Order Fire Effects Model: FOFEM 4.0, User's Guide*, U.S. For. Serv., U.S. Dep. of Agric., Washington, D. C.

Roy, D. R., L. Boschetti, and S. N. Trigg (2006), Remote sensing of fire severity: Assessing the performance of the Normalized Burn Ratio, *IEEE Geosci. Remote Sens. Lett.*, *3*(1), 112–116, doi:10.1109/LGRS.2005.858485.

Ryan, K. C. (2002), Dynamic interactions between forest structure and fire behavior in boreal ecosystems, *Silva Fenn.*, *36*(1), 13–39.

Sedano, F., and J. T. Randerson (2014), Multi-scale influence of vapor pressure deficit on fire ignition and spread in boreal forest ecosystems, *Biogeosciences*, *11*(14), 3739–3755, doi:10.5194/bg-11-3739-2014.

Shen, S., G. Badhwar, and G. Carnes (1985), Separability of boreal forest species in the Lake Jennette Area, Minnesota, *Photogramm. Eng. Remote Sens.*, *51*(11), 1775–1783.

Shetler, G., M. R. Turetsky, E. S. Kane, and E. Kasischke (2008), Sphagnum mosses limit total carbon consumption during fire in Alaskan black spruce forests, *Can. J. For. Res.*, *38*(8), 2328–2336, doi:10.1139/X08-057.

Sorbel, B., and J. Allen (2005), Space-based burn severity mapping in Alaska's National Parks, *Alsk. Park Sci.*, *4*(1), 5–11.

Soverel, N. O., D. D. B. Perrakis, and N. C. Coops (2010), Estimating burn severity from Landsat dNBR and RdNBR indices across western Canada, *Remote Sens. Environ.*, *114*(9), 1896–1909, doi:10.1016/j.rse.2010.03.013.

Stocks, B., B. Lawson, M. Alexander, C. Vanwagner, R. Mcalpine, T. Lynham, and D. Dube (1989), The Canadian forest fire danger rating system—An overview, *For. Chron.*, *65*(6), 450–457.

Stocks, B. J. (1987), Fire behavior in immature jack pine, *Can. J. For. Res.*, *17*(1), 80–86, doi:10.1139/x87-014.

Stocks, B. J. (1989), Fire behavior in mature jack pine, *Can. J. For. Res.*, *19*(6), 783–790, doi:10.1139/x89-119.

Stocks, B. J., and J. B. Kauffman (1997), Biomass consumption and behavior of wildland fires in boreal, temperate, and tropical ecosystems: Parameters necessary to interpret historic fire regimes and future fire scenarios, in *Sediment Records of Biomass Burning and Global Change*, edited by J. S. Clark et al., pp. 169–188, Springer, Berlin.

Stocks, B. J., et al. (2003), Large forest fires in Canada, 1959–1997, *J. Geophys. Res.*, *108*(D1), 8149, doi:10.1029/2001JD000484.

Stocks, B. J., et al. (2004), Crown fire behaviour in a northern jack pine-black spruce forest, *Can. J. For. Res.*, *34*(8), 1548–1560, doi:10.1139/X04-054.

Stroppiana, D., S. Pinnock, J. M. C. Pereira, and J. M. Gregoire (2002), Radiometric analysis of SPOT-VEGETATION images for burnt area detection in Northern Australia, *Remote Sens. Environ.*, *82*(1), 21–37, doi:10.1016/S0034-4257(02)00021-4.

Tan, B., R. Wolfe, J. Masek, F. Gao, and E. F. Vermote (2010), An illumination correction algorithm on Landsat-TM data, in *Geoscience and Remote Sensing Symposium*, pp. 1964–1967, IEEE International, Honolulu, HI.

Trigg, S., and S. Flasse (2000), Characterizing the spectral-temporal response of burned savannah using in situ spectroradiometry and infrared thermometry, *Int. J. Remote Sens.*, *21*(16), 3161–3168, doi:10.1080/01431160050145045.

Turetsky, M. R., M. C. Mack, J. W. Harden, and K. L. Manies (2005), Spatial patterning of soil carbon storage across boreal landscapes, in *Ecosystem Function in Heterogeneous Landscapes*, edited by G. M. Lovett et al., pp. 229–255, Springer, New York.

Turetsky, M. R., E. S. Kane, J. W. Harden, R. D. Ottmar, K. L. Manies, E. Hoy, and E. S. Kasischke (2011), Recent acceleration of biomass burning and carbon losses in Alaskan forests and peatlands, *Nat. Geosci.*, *4*(1), 27–31, doi:10.1038/NGEO1027.

U.S. Department of Interior, Geologic Survey (2009), LANDFIRE: LANDFIRE existing vegetation type layer. [Available at www.landfire.gov.] (Accessed 16 April 2012).

Ung, C.-H., P. Bernier, and X.-J. Guo (2008), Canadian national biomass equations: New parameter estimates that include British Columbia data, *Can. J. For. Res.*, *38*(5), 1123–1132, doi:10.1139/X07-224.

USGS (U.S. Geological Survey) (2012), GLOVIS website. [Available at http://glovis.usgs.gov/.] (Accessed 15 November 2012).

Van der Werf, G. R., J. T. Randerson, L. Giglio, G. J. Collatz, M. Mu, P. S. Kasibhatla, D. C. Morton, R. S. DeFries, Y. Jin, and T. T. van Leeuwen (2010), Global fire emissions and the contribution of deforestation, savanna, forest, agricultural, and peat fires (1997–2009), *Atmos. Chem. Phys.*, *10*, 11,707–11,735.

Van Wagtendonk, J. W., R. R. Root, and C. H. Key (2004), Comparison of AVIRIS and Landsat ETM + detection capabilities for burn severity, *Remote Sens. Environ.*, *92*(3), 397–408, doi:10.1016/j.rse.2003.12.015.

Veraverbeke, S., and S. J. Hook (2013), Evaluating spectral indices and spectral mixture analysis for assessing fire severity, combustion completeness and carbon emissions, *Int. J. Wildland Fire*, *22*(5), 707–720, doi:10.1071/WF12168.

Veraverbeke, S., W. W. Verstraeten, S. Lhermitte, and R. Goossens (2010a), Evaluating Landsat Thematic Mapper spectral indices for estimating burn severity of the 2007 Peloponnese wildfires in Greece, *Int. J. Wildland Fire*, *19*(5), 558–569, doi:10.1071/WF09069.

Veraverbeke, S., W. W. Verstraeten, S. Lhermitte, and R. Goossens (2010b), Illumination effects on the differenced Normalized Burn Ratio's optimality for assessing fire severity, *Int. J. Appl. Earth Obs. Geoinf.*, *12*(1), 60–70, doi:10.1016/j.jag.2009.10.004.

Verbyla, D., and R. Lord (2008), Estimating post-fire organic soil depth in the Alaskan boreal forest using the Normalized Burn Ratio, *Int. J. Remote Sens.*, *29*(13), 3845–3853, doi:10.1080/01431160701802497.

Viereck, L. A. (1983), The effects of fire in black spruce ecosystems of Alaska and northern Canada, in *The Role of Fire in Northern Circumpolar Ecosystems*, edited by R. W. Wein and D. A. Maclean, pp. 201–220, Wiley, New York.

Welp, L. R., J. T. Randerson, and H. P. Liu (2007), The sensitivity of carbon fluxes to spring warming and summer drought depends on plant functional type in boreal forest ecosystems, *Agric. For. Meteorol.*, *147*(3–4), 172–185, doi:10.1016/j.agrformet.2007.07.010.

Wirth, C. (2005), Fire regime and tree diversity in boreal forests: Implications for the carbon cycle, in *Forest Diversity and Function*, edited by D. M. Scherer-Lorenzen, P. D. C. Körner, and P. D. E.-D. Schulze, pp. 309–344, Springer, Berlin Heidelberg.

Yarie, J., and K. Vancleve (1983), Biomass and productivity of white spruce stands in interior Alaska, *Can. J. For. Res.*, *13*(5), 767–772, doi:10.1139/x83-106.